Memoirs of the Faculty of Engineering, Nagoya University
Vol. 31, No. 1. (1979)

INVESTIGATION INTO THE SHEARING PROCESS OF DUCTILE SHEET METALS

YASUO KASUGA, SHIGEAKI TSUTSUMI and TOSHIHIKO MORI

Department of Mechanical Engineering

(Received June 1, 1979)

Abstract

This paper presents a comprehensive view of the shearing procedure attained by detailed observations.

In order to provide a fundamental approach to blanking operation in general a simplified shearing model with scissors-like tools is proposed and treated in detail in the first half of this research. According to this model, the penetration of the tool can be resolved into three imagined constituent components, and by means of this resolution, a new interpretation of the shearing performance has become possible. The same model is analyzed theoretically in which slip-line solutions consistent both kinematically and statically could be proposed. The phenomena occurring in various blanking processes will be adequately understood by taking account of their own external constraints and so modifying the scissors type shear.

In the latter half, behavior of metal in the circular blanking has been investigated. A particular visioplasticity and a strain gauge method are employed for the observations of material flow. It has been found that the time when the ultimate crack initiates depends on the discontinuity of average radial velocities of material across a boundary of the product and the scrap.

Contents

Nomenclature

(*1*) *Symbols which appear in Part* Ⅰ *and* Ⅱ

Referring to Fig. 1, the symbols are defined as follows;

t_0 : thickness of material
s : tool advancement, penetration
c : clearance

w : cotact width (the contact area on the tool face divided by the profile length)

a : contact width (on the tool mantle face)

ω : rotative displacement of rigid parts of the material

l : gauge length measured in the longitudinal direction of the specimen (the fiducial grid lines being marked on both rigid parts)

h : step of the rigid parts produced by shifting motion of the material measured normal to the general surface of the material

f : indentatation of the tool into the material

$e=t_0-s$: vertical gap of both cutting edges

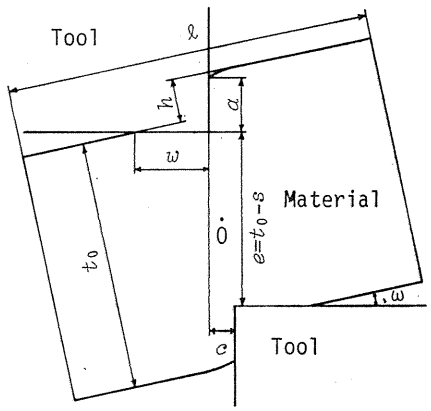

Fig. 1. Definition of symbols.

Symbols of the calculated values are defined as follows.

s_1 : "effective shear component" of the tool advancement

s_2 : "indentation component" of it

s_3 : "rigid body rotaiton component" of it

$l-l_0$: separation of the rigid parts, that is, the elongation of the gauge length in the longitudinal direction.

Specific value of length relative to the material thickness t_0 is denoted by adding a bar above the letter, e. g., the non-dimensional value of w is $\bar{w}$.

As to the forces, the following symbols are used. (ref. Fig. 2)

p_0 : hydrostatic pressure prevailing in the material

p_V : pressure on the tool face

p_H : pressure on the tool mantle face

T_V : frictional force on the tool face per unit profile line length

T_H : frictional force on the tool mantle face per unit profile line length

$\tau_V=k\cdot\cos 2\gamma$: frictional shear stress on the tool face

$\tau_H=k\cdot\cos 2\delta$: frictional shear stress on the tool mantle face

γ, δ : inclination of the β-shear line to the tool face

k : yield stress in simple shear

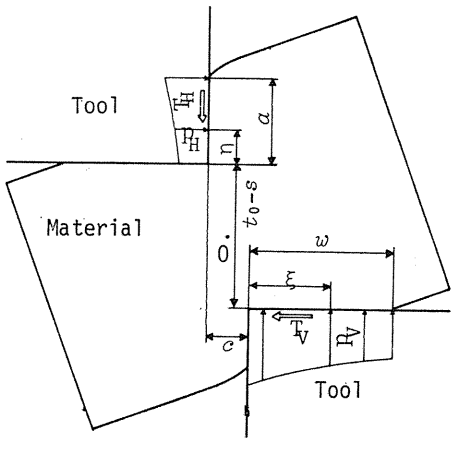

Fig. 2. External forces acting on the material.

(2) Symbols used in Part Ⅲ

ε_r, ε_θ : radial and tangential strains in cylindrical coordinates

θ : the inclination of originally horizontal grid line in the meridio-sectional plane of the material

r, z : radial and axial coordinates on the meridio-sectional plane

u : radial displacement of the material

$v=\partial u/\partial s$: radial flow of it, where $\frac{\partial u}{\partial s}=\frac{\partial u/\partial \tau}{ds/d\tau(=\text{punch speed})}=\text{const.}\times\frac{\partial u}{\partial \tau}$ ($\tau=$time)

$\bar{v}$: average radial velocity over the thickness

v^* : the discontinuity of $\bar{v}$s between the scrap side and the product side estimated by extrapolations of their radial distributions, a measure which expresses the flow into or out of the clearance zone.

Introduction

In those days when the shearing was regarded simply as a preparatory process of material-separation, it was thought that the optimum condition of the process would be attained by making two cracks which start from upper and lower cutting edges to meet together so as to make the work required minimum as well as to give a good finish to the surface separated.[1~3] Recently however, with an increasing demand for the functional accuracy of a sheared component, it has become important to make the sheared surface square and to have enough dimensional accuracy.[4~10] Thus, due to the natural multiplicity of the aim of the processing as well as the difficulty in the analysis of an unsteady deformation in a very confined zone of the material and that of a fracture which follows, papers published which could give a general and unified view of the process seem scarce.[11~27]

In order to understand the shearing phenomenon comprehensively and systematically, it would be useful to grasp the deformation referring to some typical models. In this research, as the most basic type of shearing a model of the "scissors type" shear is considered where a sheet metal is severed by nipping it with two cutting edges only, otherwise unconstrained. If in a practical operation the external constraints imposed on the material were removed as far as possible, namely, if the process were wholly conducted by an upper and a lower straight cutting edges only, the process would make the material to deform as to keep the work necessary minimum, Though this type of shearing would be regarded as of typical, it could include fundamental phenomena in many shearing processes of practical use. Thus, detailed observation and a suitable analysis of the "scissors type" shear are considered useful to attain an essential view about the basic mechanism of deformation and fracture in the process in general. The phenomena occurring in various shearing processes, which include shearing with straight blades, profile blanking, finish blanking, bar cropping and so forth, would be adequately understood by taking account of their own external constraints in excess and so modifying the scissors type. In view of the similar understanding, Тимощенко (1977) said that in order to understand the shearing phenomenon systematically the constraints imposed on the material in the process should be considered.[28]

The observation of the deformation along with this line has been carried out on some plastic model material and alminium sheet metals where a photoetched grid method were employed. Thus, characteristic features in this type of shearing have been clarified for the first time. This will be referred to in Part I. In this part, it is clarified that allowable rotation of material peculiar to this type makes the tool to indent more easily by shifting two portions of material. As to characterize the sequence of deformation, increments of the tool advancement were

considered as composed of three components. And, it was thought that balance of these components could determine the process performance.

In view of this new approach mentioned in Part Ⅰ, an attempt to establish the kinematics of this process were made, its result being presented in Part Ⅱ. In this theory kinematically and statically consistent slip-line solutions are proposed. They deal with the four discriminating stages in a process, and four kinds of the fields thus obtained could be joined each other without any abruptness. On the basis of the proposed fields meaning of each resolved component above stated is explained. Thus it has become possible to estimate the process of punch load as well as the width of contact zone.

In a blanking of sheet metals, the material undergoes more constraints than in the "scissors type" and so the behavior of material appears to depend on the severity of these constraints. In this view point, Part Ⅲ refers to the mechanism of the circular blanking. In this part also, observation of the material behavior during a process is presented. But, since a blanked component usually takes a closed contour, the existence of the contour's curvature makes the process more complicated.[15, 20, 29~31] So, difficulty in analysis arises partly from the preparation of test specimens which can be sectioned and reassembled in order to observe the deformation grid during the process.

In this investigation, by employing a visioplasticity and a strain gauge method the flow of metal during the blanking of closed contours could successfully be studied. The procedure of circular blanking has been clarified on the basis of the knowledge of this metal flow throughout the deforming zone.

After all, the whole schedule of this investigation aims at a comprehensive view of the shearing including blanking and piercing.

Part Ⅰ. Experiment on the Scissors Type Shear [32]

1. Introduction

In this part, an experimental result on the "scissors type shear" of aluminium piece is presented. The process, from the beginning to the stage of crack initiation in the material, was observed closely. With this observation, it was proved that this type could show a representative pattern of material behavior essential to the shearing in general.

It has also been clarified that the advancement of the tool can be imagined to cause the rigid body rotation of the material as a whole, the relative shift and the indentation. The existence of the rigid body rotation is significant due to its facility in advancing the tool. Further, a new interpretation of the shearing performance according to the ratios of these three component displacements has been suggested.

2. Condition of Expeirment and Method

Aluminium metal pieces of 4.0 mm thick, 60 mm width and 60 mm length were cut from the sheets of standard size and tested by the scissors type shearing with

an experimantal tool set which was composed of an upper punch having double straight edges and a suitable lower die. In order to visualize the deformation during a process, test pieces were cut lengthwise into halves and a square grid of 0.5 mm mesh was photoetched on one sectional plane.

Scissors type shearing was realized by splitting the test pieces further into halves at the middle of their length. Table 1 shows the condition of experiment and Table 2 the mechanical properties of test sheet.

Fig. 3 shows a sheme of the experimental tool set where ① indicates the upper punch, ② the test specimen and ③ the lower die. In accordance with the lengthwise division of the specimens a split construction into halves is adopted each for the punch and for the die. At any instant of interest in a process, the driving unit

Table 1. Experimental condition.

Tool	Tool angle : 90° Material : SKD 11 Hardness (HRc) : 60～62 Roughness (Ra) : 0.02 μm
Shear type : Scissors	
Clearance : 5%, 10% and 15% of specimen thickness	
Lubricant : Johnsonwax No. 151	
Punch speed : 0.25mm/sec	
Temperature : 20～24°C	
Humidity : 52～60%	

Table 2. Mechanical properties of test sheet.

Material : Aluminium (A 1100 P-H 14)
Dimension : 4.0mm×60.0mm×60.0mm
Hardness (Hv) : 33.6
0.2% proof stress : 10.20kgf/mm^2
Ultimate strength : 10.83kgf/mm^2
Strain hardening exponent : 0.031
Uniform elongation : 3.2%
Elongation : 15.0%
Reduction of area : 56.8%

can be stopped and the front half of the tool set was wholly removed from the position so as to reveal the grid on the sectional plane and its distorted geometry at that instant is photographed.

The punch holder ⑥ is connected to the elastic diaphragm of a force-measuring unit inserted in the force-transmission system. Deflection of the diaphragm is detected by foil strain gauges attached on it whose output was calibrated by known loads.

Fig. 4 shows the load diagram of an interrupted and repeated process. In this figure, if the second interruption point at *dn*, for instance, is a moment of interest, the machine is stopped at *dn* and after the unloading of *dn* to *st* a grid photograph is taken.

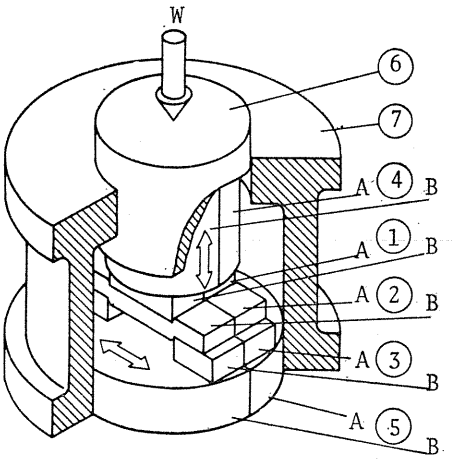

1. punch edge 2. specimen
3. die edge 4. punch shank
5. die bolster 6. punch slide
7. frame

A. rear half B. front half

Fig. 3. Scheme of experimental tool set

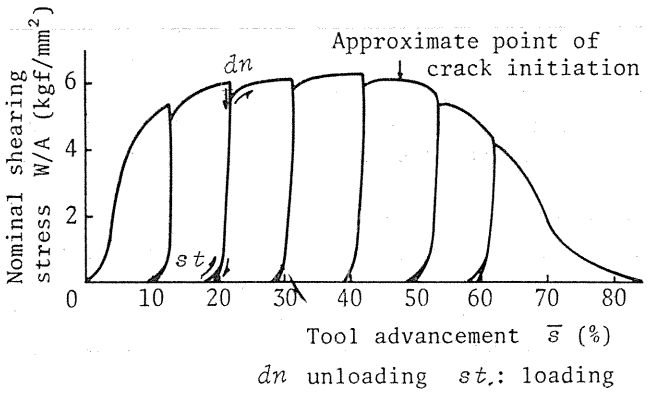

Fig. 4. Load diagram of interrupted and repeated process.

3. Result and Consideration

Fig. 5 shows three patterns of deformation observed as typical in shearing processes. (**a**) is the scissors type, (**b**) the shearing by the constrained scrap ends

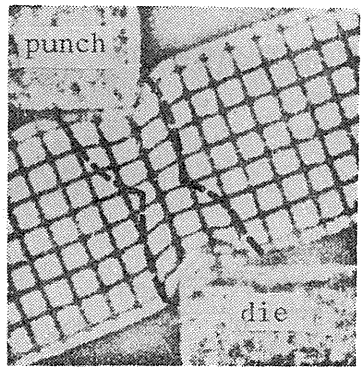

(a) Scissors type

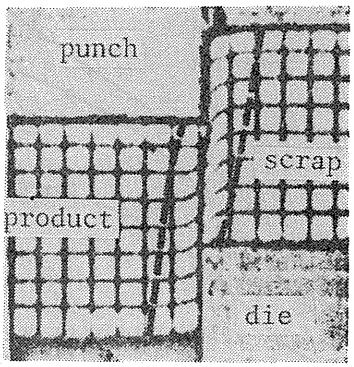

(b) Shearing by constrained scrap ends

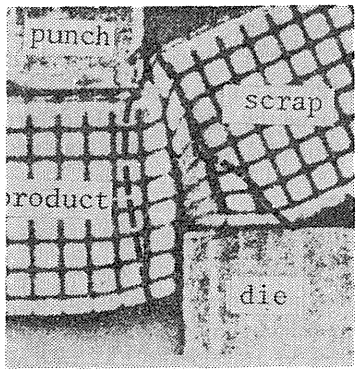

(c) Shearing by unconstrained scrap ends

Fig. 5. Three patterns of deformation observed as typical in shearing processes.

and (**c**) the blanking by the unconstrained scrap ends. It will be seen that the blanking in general which resembles the case of (**c**) is a mixture of (**a**) and (**b**).

The dashed lines in the figure are the borders of the deformed zones on rigid zones. They were estimated by overlapping the negative films taken at neighbouring two stages and by matching the grids of their undeformed portion.[33]

3. 1. Process of the scissors type shearing

Fig. 6 shows the development of inclination of the rigid zone during a process. At start, as the punch advances, the material in that portion seems to rotate wholly and almost abruptly, keeping itself rigid, to an inclination of prescribed amount which depends on the tool clearance c and the thickness t_0 as follows;

$$\omega_s = \sin^{-1}(c/t_0).$$

At the end of this rigid rotation as a whole, advancement of the punch is only

$$s = t_0\{1-\sqrt{1-(c/t_0)^2}\}.$$

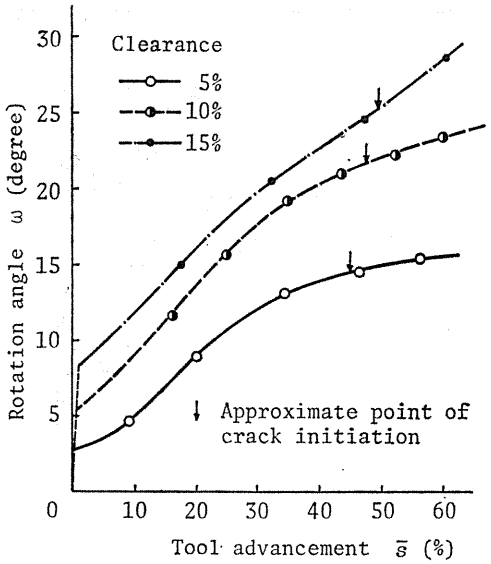

Fig. 6. Development of inclination of rigid zone of material during a process.

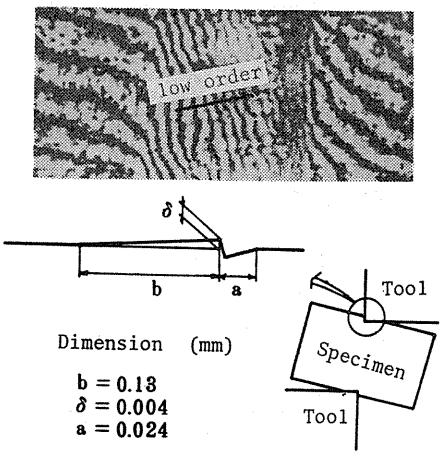

Fig. 7. Piling up of surface material, proved by means of interference fringe pattern taken from surface.

The stage which follows is the indentation of the cutting edge into material. This causes a superficial plastic deformation and the rotation as a whole seems virtually to cease. Fig. 7 shows a slight piling up of the surface material at this stage being proved by means of the interference fringe pattern taken from the surface. Fig. 8a shows the possible deformation zones at this stage. As the punch advances, the material continues to rotate wholly, two portions of it being squeezed by the tools.

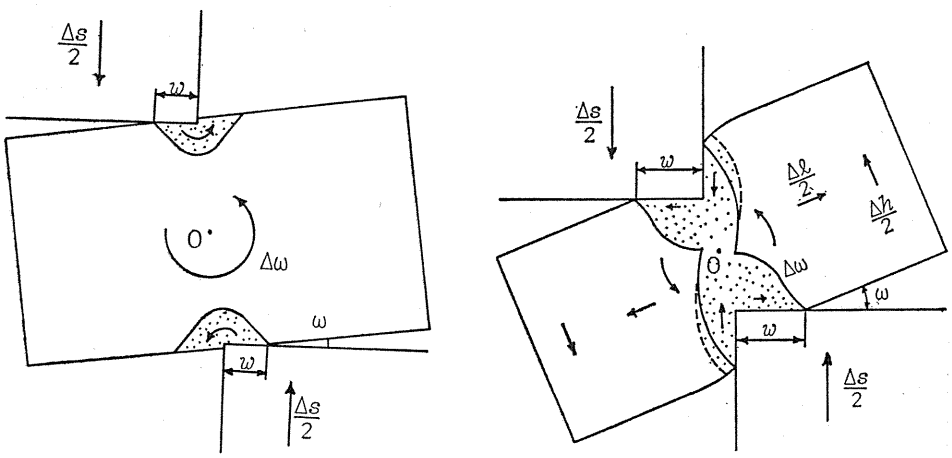

(a) (b)

ω : Rotation angle
w : Contact width
Δs : Increment of tool advancement
Δl : Increment of separation
Δh : Increment of step

Fig. 8. Possible deformation zones at two stages in scissors type shearing.

Fig. 9 shows the increase of contact width w caused by penetraton of the tools during a process. As will be expected, it increases abruptly at the beginning of the deformation, but thereafter gradually. The value w at the changing point from abrupt to gradual can be estimated theoretically, which will be referred to in the next part.

When $w/(t_0-s)$, — the ratio of the contact width and the vertical gap of the edges —, reaches a particular value determined by clearance and lubrication, the plastic deformation zones, originating from both edges, become united, and penetrate through the material as shown in Fig. 8b.

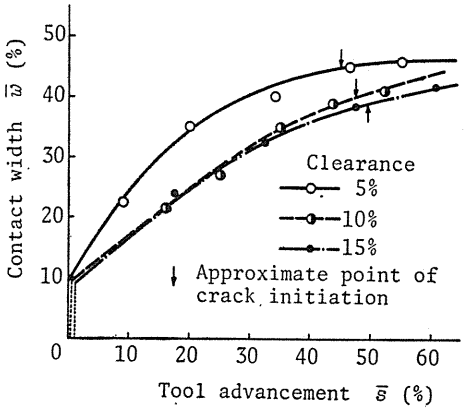

Fig. 9. Process of contact width w.

At the beginning of this stage, the surface of the material between two boundaries shown by the full and the broken lines in this figure roll over.

Through this main deformation stage during which the plastic zone spreads over the thickness of the material, the rigid parts of the material existing at both ends separate away (the separation in the longitudinal direction of the specimen is denoted by Δl) and at the same time shift one another (the step measured in the normal direction, Δh). During this stage, the rotation of the rigid parts ever continues, as shown in Fig. 6.

Fig. 10 shows the separation of the rigid zones after this stage. This is taken from the grid points in the observed section. It has been proved that, the smaller the clearance, the earlier the separation occurs.

The step h made by the material shifting naturally increase with the advancement, as shown in Fig. 11.

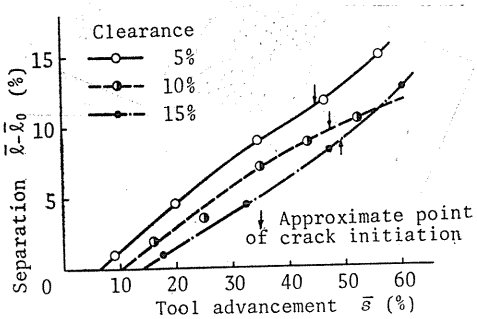

Fig. 10. Separation on rigid zones.

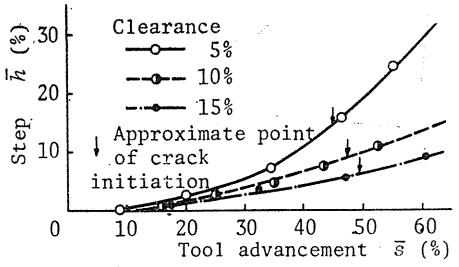

Fig. 11. Step made by material shifting.

In Fig. 9, it is shown that, whereas the curve for the case of a clearance of 5 % increases more rapidly at the beginning, it approaches to the other curves in the ultimate. Cause of this tendency will be explained theoretically in the next part.

3. 2. Role of the rotative displacement in the deformation of material

According to the preceding section it is evident that the rotation of the material against the tool is a characteristic feature of this shearing process. Thus in this section how the existence of this rotation influences the shearing mechanism will be explained, on the basis of certain sharing models proposed.

The vectors, shown in Fig. 12 and 13, represent the velocities of tools and the rigid parts of the material with respect to the origin O which are imagined at stages of Fig. 8 a and 8 b respectively.

The hodographs in the cases of Fig. 8 a and 8 b will be classified respectively into certain versions according to the extreme deformation patterns.

In Figs. 12 and 13, the symbols utilized are defined as follows;

Δs : vertical increment of the relative displacement of upper and lower tools,

$\Delta\omega$; the increment of rotative displacement of rigid parts in the material,

Δf : the vertical increment of indentation of the tool

(when the rotative displacement

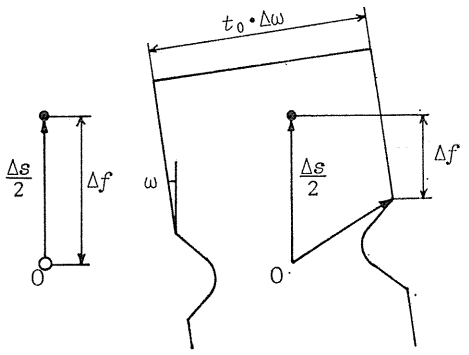

(Ⅰ) without a rigid body rotation (Ⅱ) with a rigid body rotation

Fig. 12. Velocities of tools and rigid parts of material with respect to origin O which are imagined at stage of Fig. 8 (a).

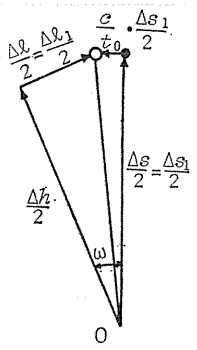

(Ⅰ) no a plastic indentation, no rolling over and no rigid body rotation

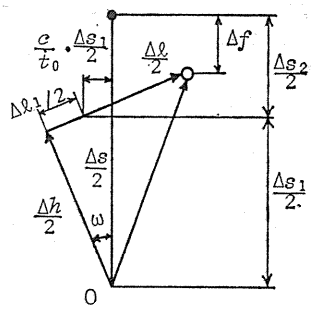

(Ⅱ) the indentation and the rolling over except a rotation

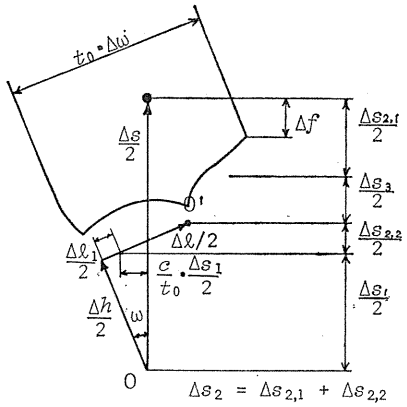

O′ : Virtual velocity in the right rigid zone when it extends to the position O

(Ⅲ) the all possible displacements exist

Fig. 13. Velocities of tools and rigid parts of material with respect to origin O which are imagined at stage of Fig. 8 (b).

exists in a hodograph, the velocity at the border end of tool-material contact is taken as representative.),

Δl : the increment of the separation of the rigid parts (in the longitudinal direction of the specimen),

Δh : the increment of the step of the rigid parts (measured normally to the general surface of the material).

The deformation patterns possible in each case are assumed as follows.

In the case of Fig. 12 the deformations are classified into (Ⅰ) one without a rigid body rotation and (Ⅱ) one with rotation.

In the case of Fig. 13 the deformation would be possible in either of the following types; (Ⅰ) no plastic indentation under the tools, no rolling over of the free surfaces and no rigid body rotation exist (only the separation and the step making displacement exist); (Ⅱ) the indentation and the rolling over except a rotation exist; (Ⅲ) all the possible displacements exist.

In (Ⅰ) of Fig. 12 the velocity of the lower tool is indicated by black circle and that of the rigid part by white circle (which coincides with the origin O in this

case). In (Ⅱ) of Fig. 12 the velocity of the rigid part is represented by its border shape because of its rigid body rotation.

In constructing Fig. 13, it is assumed that the rigid parts of the material can move horizontally by $c \cdot \Delta s_1/2t_0$ so as to bring about a movement to fill the clearance zone.

By comparison of the deformations with and without a rotation, it will be clarified that an existence of rotation makes the indentation and the shift easy so to minimize work done by the tools.

Therefore, it is supposed that the real deformation of the scissors type shearing would occur under the condition of (Ⅱ) in the case of Fig. 12 or (Ⅲ) in Fig. 13.

3. 3. *Interpretation of the deformation mode (Resolution of the tool penetration into the constituent components)*

From the above-stated consideration, it would be said that the deformation of the scissors type shearing does not occur under a pure shift only nor under a pure indentation only, which latter case, by two opposed knife edges, has been studied by Tamura *et al.*[34], but it occurs under a mixed condition of the aboves together with a rotation. Thus, a process seems to so develop as to minimize the necessary work by making these typical deformations coexist.

So, in order to grasp the performance of a shearing process systematically, it would be useful to realize how these typical deformations play parts and in what ratio they occur in generating a sheared surface.

In the following, an analysis of the constituent components of tool advancement will be explained. The step Δh or the separation Δl, which is imagined to take place incrementally in a real shearing operation, should always be smaller than that in the extreme case where the process develops by indentation only or by step only. In this analysis, an increment of the punch advancement was thought to consist of the following increments which could be calculated from the experimental values of Δs, ω and Δh; i. e. the "effective shear component" Δs_1, which is a supposed advancement of the tool by solely making the step, the "indentation component" Δs_2, that of the tools by solely pushing its way through material and the "rigid body rotation component" Δs_3. A knowledge of the proportion of these components during a process would make it possible to characterize the shearing performance because one can discriminate the deformation mode by ratios of them.

If it can be imagined that a deformation takes place by individual constituent increments Δs_1 etc. each, the material would be effected as follows. The "effective shear component" Δs_1 would contribute to bringing about the macro-shear which is the essential purpose of the operation, namely concentration of the strain rate in the clearance zone. The "indentation component" Δs_2 would contribute to the penetration of tools through the thickness of material, and determine the distribution of the hydrostatic pressures in the thickness direction. The "rigid body rotation component" Δs_3 would facilitate the shearing process by minimizing material deformation as mentioned before. These typified properties of constituent increments are enumerated in Table 3.

Referring to the hodograph in Fig. 13 (Ⅲ), Δs_1 will be obtained by the following equation in which the experimental values of Δh, ω and c are considered to be given.

Table 3. Explanation of deformation mode
(analysis of constituent components of an incremental advancement of tool)

Component	Δs_1 (Effective shear)	Δs_2 (Indentation)	Δs_3 (Rigid body rotation)
Feature	This component constitues the macro-shear in accordance with the essential purpose of the shearing, namely concentration of the strain rate in the clearance zone.	This component constitutes the penetration of tools through the thickness of material. It determines the distribution of the hydrostatic pressures in the thickness direction.	This component has the property that facilitates the shearing process by minimizing the material deformation.
Diagram	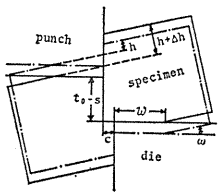	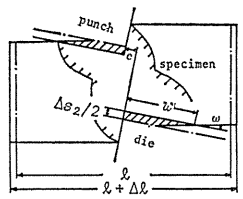	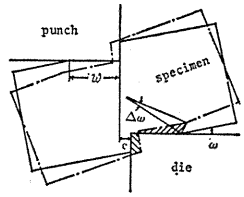
Equation	$\Delta s_1=\dfrac{\Delta h-\frac{c}{t_0}\cdot\Delta s_1\cdot\sin\omega}{\cos\omega}$	$\Delta s_2=\left(\Delta l-\dfrac{\Delta h\cdot\sin\omega-\frac{c}{t_0}\cdot\Delta s_1}{\cos\omega}\right)\dfrac{t_0}{w}$	$\Delta s_3=\Delta s-(\Delta s_1+\Delta s_2)$

$$\Delta s_1=\Delta h/\left(\cos\omega+\frac{c}{t_0}\sin\omega\right) \tag{1}.$$

As shown in Fig. 13 (I), in spite of the fact that the indentation Δf does not exist, a slight separation Δl_1 occurs according to the inclination ω of the material as tool advances by Δs_1. Thus, to attain the "indentation component" Δs_2, the separation which is the above Δl_1 subtracted from the real value of Δl should be considered in order to compensate for the pushed-through volume indicated by shaded area in the figure of the column Δs_2 of Table 3. So, Δs_2 would be able to be calculated by the following equation.

Since the pushed-through volume is:

$$A=\Delta s_2\cdot w=\{\Delta l-\left(\Delta h\cdot\sin\omega-\frac{c}{t_0}\Delta s_1\right)/\cos\omega\}t_0,$$

$$\Delta s_2=\left\{\Delta l-\Delta h\left(\frac{t_0\cdot\tan\omega-c}{t_0+c\cdot\tan\omega}\right)\right\}\frac{t_0}{w} \tag{2}.$$

Finally, the "rigid body rotation component" Δs_3 is obtained by subtracting the so far estimated two components from Δs.

Fig. 14 shows in what proportion Δs_1, Δs_2 and Δs_3 calculated by above equations change as the tool advances, where a clearance of 5 % is taken as an example.

As the tool advances, the following processes are experienced. In the rigid body rotation stage immediately after the process beginning, the tool can advance by leaning on Δs_3 only. From the beginning of the deformation stage, Δs_2 occupies the most part of Δs. For a while after that, the indentation Δs_2 continues to dominate the others. When the tools get at nearly 40% of the thickness, Δs_1 comes to about 80% of Δs, and soon after a stage of 45%, a crack initiates in the meterial neighbouring to the cutting edges, and during its propagation, $\Delta s \simeq \Delta s_1$.

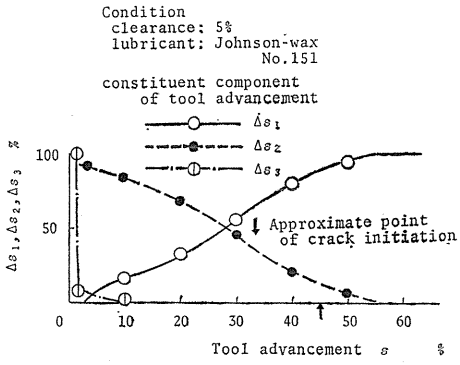

Fig. 14. Change of proportion Δs_1, Δs_2 and Δs_3 as tool advancement.

This type of analysis, in which, by resolving the tool advancement into three components, the deformation mode in a shearing was typified would be applicable to any shearing process other than the scissors type. It will be thought that change of the ratios of the components may be replaced by change of the constraint which will be exercised in the general shearing operations.

The axi-symmetrical blanking was dealt with in Part Ⅲ, and it will be clarified that the constraint of the material movement in the radial direction controls the deformation mode. In this case, material separation Δl could not take place easily because of the difficulty existed naturally in a centripetal or a centrifugal movement. And so the material becomes more constrained than in a straight scissors type shearing. Thus, to what degree this constrained radial flow is admitted in a blanking is important in considering the shearing performance. This point of view relates closely to how much of the tool advancement was possible by an indentation Δs_2 in a scissors type shearing. Further, the rising of the scrap end off the tool face and the warping of the product, which always accompany with the blanking, are nothing but versions of the rigid body rotation Δs_3.

3. 4. Relation between the load diagram and the balance of the tool advancement components

In this section, it will be shown that in the practical scissors type shear the increase of the working load with tool advancement would be less than either of those in the imagined shear carried out only by the shift Δs_1 or the indentation Δs_2.

Fig. 15 shows the load diagram, where 5% of clearance is taken as an example. Now, looking on the load diagram in the vicinity of the penetration of s_a, the load curve by a further incremental advancement of Δs at this penetration would be the one shown magnified as a solid line in Fig. 16. Supposing that at this instant of s_a, the advancement components to be $\Delta s_3 \simeq 0$ and $\Delta s_1 : \Delta s_2 = a : b$, an incremental increase of the load ΔP will cause the system to allow a total advancing of Δs which is composed of $\Delta s_1 = [a/(a+b)]\Delta s$ for the shift and $\Delta s_2 = [b/(a+b)]\Delta s$ for the indentation. As either of these components is less than Δs, compliance of the system $\Delta s/\Delta$P should be larger than either of the imagined compliances $\Delta s_1/\Delta$P and $\Delta s_2/\Delta$P. If the material is constrained so as Δs to be composed entirely of

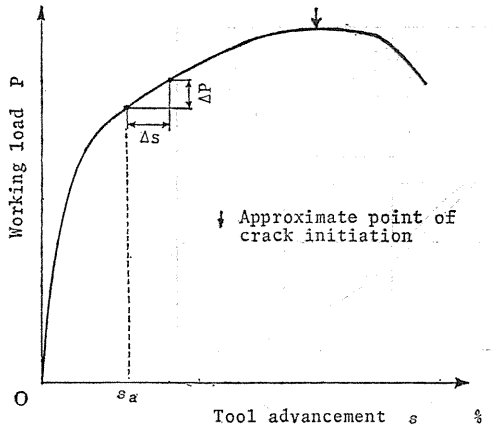

The ratios of the tool advancement components are assumed to be $\Delta s_3 \simeq 0$, $\Delta s_1 : \Delta s_2 = a : b$

Fig. 15. The load diagram drawn as a model

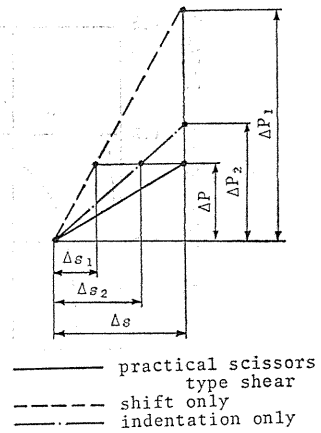

Fig. 16. The maginified load-diagram when a further incremental penetration of Δs is imposed at s_a in Fig. 15.

Δs_1, then, in accordance with the compliance $\Delta s_1/\Delta P$ the increase of the load will amount to ΔP_1 which must be larger than ΔP. The broken line in the figure shows the supposed load curve in this case.

In order to ascertain this view, the following experiment has been carried out. As shown in Fig. 17, stopper plates are attached opposite to the shearing tools, so as to limit the raising displacement of the scrap end off the tool face. In accordance with the amount of the gap between stopper and the material, so to say the

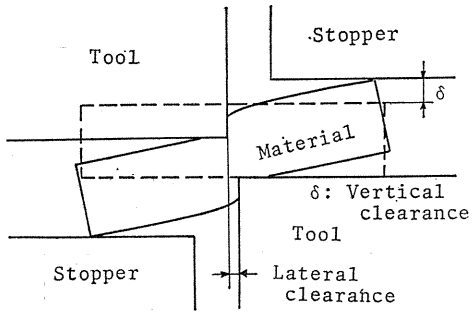

Fig. 17. The constraining device in midprocess of scissors type shear.

vertical clearance whose amount is denoted by δ in this paper, the initiation of suppressing the rigid body rotation changes. Against this vertical clearance, the usual clearance of the lateral gap between shearing tools may be said to be the lateral clearance. Fig. 18 shows the diagram of the reactive force on the stopper. In this figure, it will be noted that, the time when the scrap end begins to touch

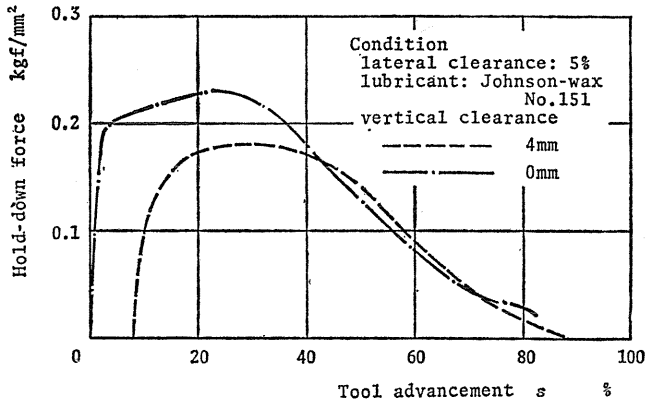

Fig. 18. The stopping force against the rigid body rotation.

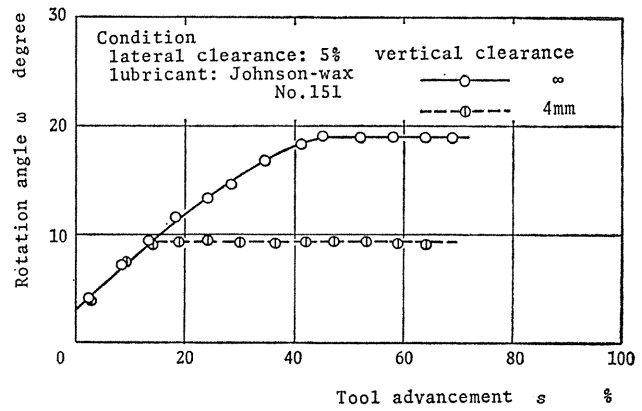

Fig. 19. Development of inclination of rigid zone of material during a process.

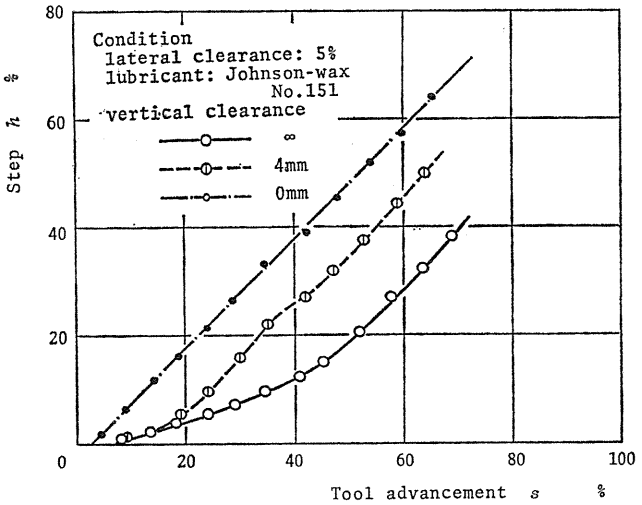

Fig. 20. Step made by material shifting.

the stopper is about 8 % in the case of $\delta=4$ mm, and thereafter the stopper continues to actuate until about 20 %. It can be seen that during this increasing process of the force the balance of the characteristics Δs_1, Δs_2, Δs_3 changes gradually so as to leave from the scissors type. The broken line in Fig. 19 shows that in the case of $\delta=4$ mm and the the lateral clearance of 5 %, the rigid body rotation ceases at the penetration of about 14 % and after that the inclined state of the scrap material becomes fixed. Similarly, as shown by the broken line in Fig. 20, after 14 % the increase rate of the step h of the material with the tool advancement comes to agree with that in the case of $\delta=0$ mm which is shown by the chain line. This means that, in the cace of $\delta=4$ mm, before the tool advancement of about 8 %, the process goes on entirely in a manner of scissors type, and after that it turns to the condition of $\Delta s \simeq \Delta s_1$, which is a type of constrained shear.

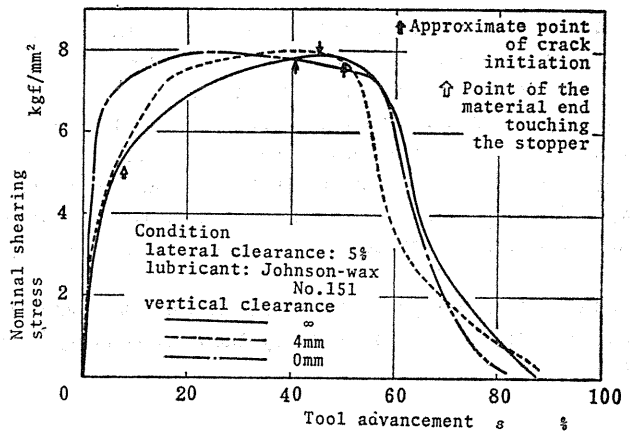

Fig. 21. The load diagram with the material constrainedin mid-process of the scissors type.

Consequently, the shearing load will increase as follows. The load curves for a common lateral clearance of 5 % but different vertical clearance of ∞, 4 mm and 0 mm, are shown by solid, broken and chain lines in Fig. 21 respectively. Before the time when the scrap end touches the stopper, the curve for $\delta=4$ mm coincides wholly with an unconstrained shear. Though the situation of the material and the accompanied plastic work agree with those of the unconstrained scissors type shear until 8 %, immediately after this time, the process turns to a constrained shear. At the stage of 8 % when the material touches the stopper, the ratios of the constituent components of the tool advancement are $\Delta s_1 : \Delta s_2 : \Delta s_3 \simeq 1 : 5 : 0$, as can be read from Fig. 14. By means of utilizing these ratios ($a : b : 0$) and the inclination $\Delta P/\Delta s$ at that stage, shown by solid line in Fig. 21, ΔP_1 and ΔP_2 could be imagined as shown in Fig. 16. The $\Delta P_1/\Delta s$ acquired in this manner coincides with the inclination $\Delta P/\Delta s$ of the load curve at the stage of 8 % in the effective shear as shown by the broken line in Fig. 21. Thus, it has been verified that ascent of the working load by the practical scissors type is less than that in the imagined shear carried out only by the shift Δs_1 or the indentation Δs_2 only.

4. Summary

In order to understand the shearing phenomena comprehensively and systematically, it was intended to grasp the deformation referring to some typical models. In that, the scissors type process is dealt with as a model deformation. On the basis of detailed observation of the deformation in this process some characteristic features are pointed out which are as follows.

(1) In order to compare deformation in the three typical shearing operations, a form of the visioplasticity is applied. It can be understood that the blanking in general represents a transition from the scissors type shearing to that of the constrained shear.

(2) The observation could prove how the process in the scissors type shearing developed.

(3) By comparison of the deformations with and without a material rotation, it is clarified that an existence of rotation makes the indentation and the shift easy and so causes an easy penetration of the tools.

(4) As a method to specify the deformation mode, an analysis is introduced in which increments of the tool advancement were resolved into the "effective shear component" Δs_1, the "indentation component" Δs_2 and the "rigid boby rotation component" Δs_3. And, it is shown that by means of the proportion of these three components the deformation characteristics in a general shearing operation can be described.

Further, in the subsequent part, it will be shown that some phenomena treated in this part can be interpreted thoroughly by theoretical analysis by means of the slip-line fields.

Part Ⅱ. Theoretical Analysis of the Scissors Type Shear[35]

1. Introduction

The kinematic analysis of the shearing originates from the time when the stress distribution in the material at the beginning of piercing was solved by Bach[36] as an elastic problem. It was succeeded by Timmerbeil[15] who dealt with the similar problem by taking account of material warping. But about twenty years since, the researches have been conducted mainly in our country.

Maeda dealt with the ordinary punch and die process regarding it as a plastic deformation process and proposed a kinematical model for the first time.[25] In this model, simple shear deformation was assumed to occur continuously in a thin straight layer terminating in the edges of punch and die. On this assumption he calculated the shearing resistence of actual sheet metals from their stress-strain curves. The error of this calculation was within about 10 % for most commercial sheet metals. Afterwards the shear models with some theoretical consistency were proposed by Jimma.[22, 23] In this theory, the process was assumed to pass through four stages of the kinematically admissible velocity fields. Whereas in Maeda's theory the material of non-deformed zone should flow normal to the shear direction

in order to fulfill the condition of continuity, in Jimma's theory the material needs not such a flow because of his skillful fields proposed; so Jimma's model seemed to be able to explain the deformation in a real process.

Recently, a shearing model was proposed by Krämer.[37] In his model, a lenticular plastic deformation zone was assumed to be coincident with the work-hardening zone in the actual process. However, this model held in case of zero clearance only.

In an actual process, however, the phenomenon is very complicated and the material is deformed usually in a strictly limited zone, so a theoretical approach to this process so far has experienced more or less difficulties in its consistency. Thus, to all above-mentioned researches without exception a rigorous plasticity theory could not be applied unless one made some assumptions which were not plausible. In other words, although any one of the proposed models so far could hold in the interpretation of the shearing phenomenon at a particular instance of the process, it is not likely to be applicable throughout a whole process.

In this part, a description is given of a consistent figure of the "scissors type" shear using slip-line fields under some assumptions for the sake of simplicity. In this analysis, the slip-line field and the relating hodograph have been newly constructed which are completely compatible with the equilibrium of external forces and of the stresses acting on the rigid portions, being given the tools advancement, clearance and frictional stress on the tool face. After all, four fields of different patterns are proposed. They can transit one by one consistently through a process offering a clear interpretation of the shearing mechanism.

Recently, some researchers proposed the slip-line fields for the bar cropping. The fields proposed by В. А. Тимощенко *et al.* are based on the Lüders' band of steel and they progress in four stages.[38] The one by D. El-Wakil is based on the visioplasticity of lead specimen using the scribed circles and progresses in two stages.[39] The fields they proposed seem similar to our proposal, but, insufficient in exactness than the ones in this paper.

By means of these fields in this paper, for example, one can forsee a change of the rigid body rotation and the difference in the contact width due to a change of the clearance. Further, as the proposed fields were so constructed as to satisfy the boundary condition of the stress on the free surface, the process of a theoretically estimated load has proved to agree well with that of the experimental load. A theoretical examination of the sequence of hydrostatic pressure near the cutting edges has shown that this pressure should come to zero immediately before a crack initiation.

Although the slip-line fields of this paper are complicated to some extent, they seem to be more rigorous in the plasticity theory than any other models so far. So, they are likely to go far toward a comprehensive understanding of the shear mechanism.

2. Assumptions

The analysis of the "scissors type" shear by means of the slip-line fields, was developed under the following assumptions.

(1) The material is isotropic, homogeneous and ideally plastic.

(2) The tool has square edges and zero shear angle.

(3) The thickness is much less than the width, so the material is plane-strained.

(4) The stress configurations in the neighbourhood of both cutting edges are similar.

3. Deformation Characteristics

3. 1. The first stage (indentation, formation of contact width)

Fig. 22 shows the slip-line field which can be assumed for the first stage. In this field, the piling up of the free surface occurs as observed in the previous part. Though the field is constructed only for the frictionless tool face for the sake of simplicity, the construction might be easily extended for a constant frictional stress on it.

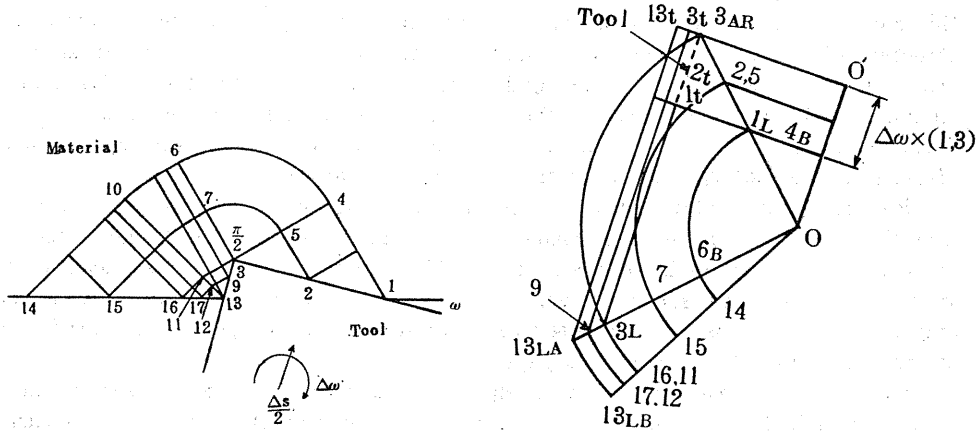

a. Physical plane b. Hodograph plane

Fig. 22. Slip-line field for the first stage (indentation).

In the hodograph plane, the material is supposed as fixed, and the tool, shown by 1·3·13 in the physical plane, displaces vertically by $\Delta s/2$ and at the same time rotates by $\Delta\omega$. So, the motion of the tool is indicated by the broken line 1t·3t·13t, and $\overline{1t\cdot 3t}$ divided by $\overline{1\cdot 3}$ represents the rotative displacement of $\Delta\omega$.

In this stage, the contact width increases very rapidly with a consequent rapid increase of the load in spite of a less increase of the pressure. When w/e, — the ratio of the contact width and the vertical gap of both edges —, reaches a particular value determined by clearance and lubrication, the deformation changes to the next stage where the increase rate of the contact width becomes smaller. So, this first stage may be called the stage of the contact width formation. It takes place instantaneously at the start of a process (see Appendix 1).

3. 2. The second stage (formation of rolling over)

Fig. 23 shows the slip-line field assumed for the second stage. Instead of the

piling up in the previous stage, the free surfaces roll over. The plastic deformation zones extended outside of 6·9·18·11 etc. which are originated from both edges (in Fig. 22 a they correspond to the zones within the curve of 1·4·6·10· 14 etc.) become united and penetrate through the material.

In the hodograph of Fig. 23 b, the stationary point corresponds to the center of the material O in Fig. 23 a, the lower and upper tools displace vertically by an amount of $\Delta s/2$ and the rotation of material 1M·1·2 ~ 6·2M is expressed by its curved shape.

The velocity of the free surface 1·7 is expressed by the broken line of $1\cdot 7_{RA}$ corresponding to the rolling over.

In this stage, the most part of Δs is occupied by the "indentation component" Δs_2 which represents the deformation in the zone within the border 2·3·4·5·6·10. And this zone is considered to be a development of the compressive deformation in the previous stage. In such a deformation, the rigid portion of material at both ends separate away in the general lengthwise direction of the specimen by Δl, which includes a little separation caused by the deformation corresponding to Δs_1.

Having recourse to the Prager's criterion[40] it was verified that the entire velocity field furnished a positive power of dissipation, although in the zone within

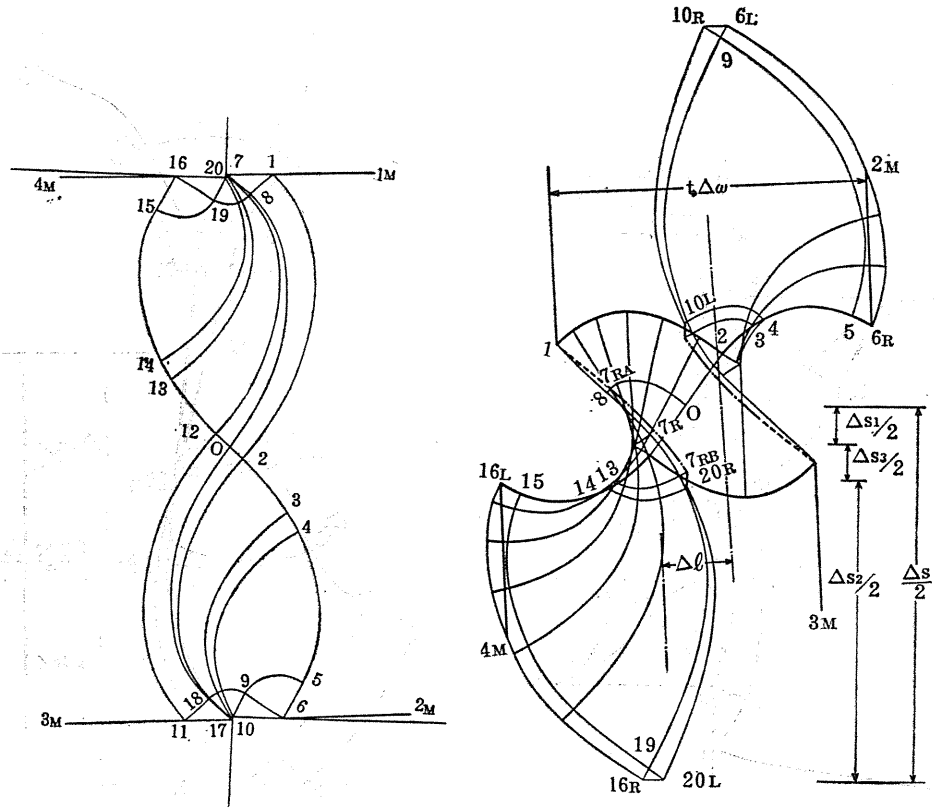

a. Physical plane b. Hodograph plane

Fig. 23. Slip-line field for the second stage (formation of a rolling over).

the border of 1·2·18·11·8 the direction of shear stress along the slip-line seems at first sight to be opposite to that of the relative velocity. This apparent discrepancy will be canceled by superposing on the whole material a rotation.

3. 3. *The third stage (main deformation)*

Fig. 24 a shows the slip-line field assumed for the third stage. Whereas in the previous stage the pressure on the tool face increases with an increase of rotation, in this stage the pressure decreases with an increase of w/e. Thus, the change of stages may be considered to occur at a particular amount of the pressure, and it will be determined by comparison of the calculated pressures in the fields of both stages.

In the hodograph plane of Fig. 24 b, the motions of tools and the material are similar to those in the previous stage. However, it was drawn for only upper half of the field, i. e., 1·N·15·18, for the sake of simplicity.

The curves of 1∼N∼8, 18∼O∼8 and 18∼N_1∼11 among β-lines are discontinuity lines, and by the aid of this band zone both rigid portions shift from one another by Δh. The deformation corresponding to the step Δh in this stage is much larger than before.

The component Δs_1, that is, the discontinuity along the line of 1∼N∼8 increases

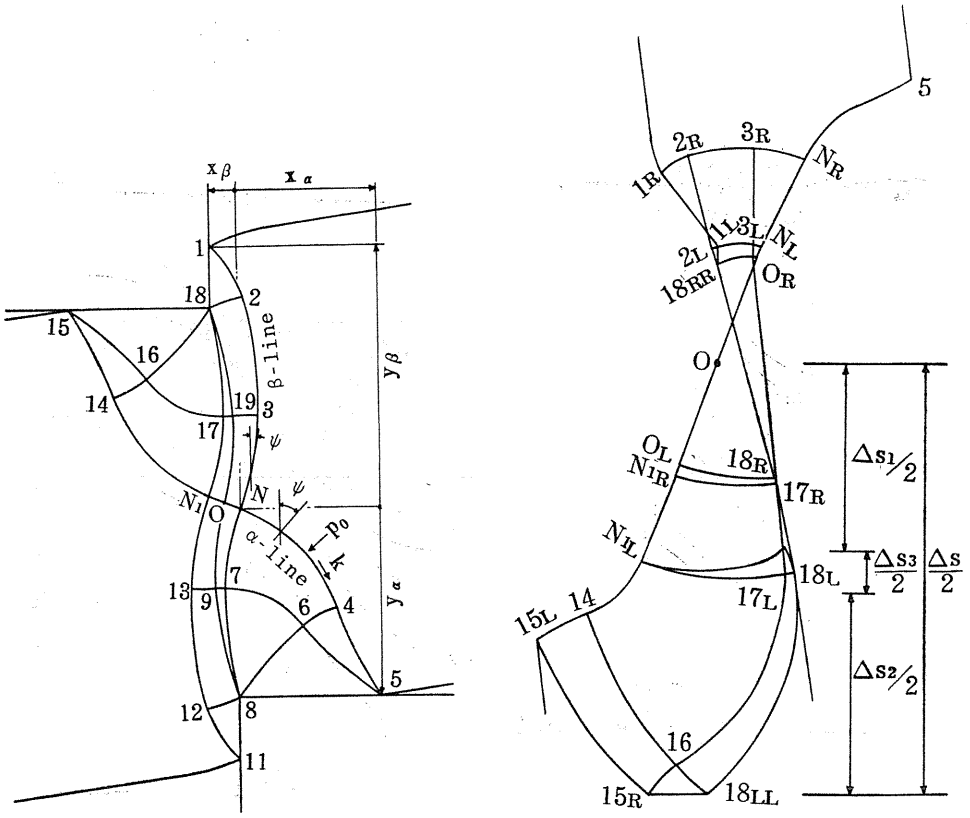

a. Physical plane b. Hodograph plane

Fig. 24. Slip-line field for the third stage (main deformation).

with the tool advancement, the reasons for this being as follows. A line segment of $1_R \cdot 1_L$ must intersect that of $2_R \cdot 2_L$ in the hodograph plane, because the downwards velocity at the point 18 must be larger than that at the point 1 according to the direction of the principal stress. Further, the mean radius of curvature of the curve 1·2 must increase, because the increase rate of the length of 1·2 is larger in comparison with that of the angle between the inclinations at the points 1 and 2.

On the other hand, the component Δs_2 must decrease with tool advancement, because the angle $\angle 14 \cdot 15 \cdot 16$ of the centered fan decreases, reflecting that the length of the curve 14·16 decreases in the hodograph plane.

3. 4. The fourth stage

Fig. 25 shows the slip-line field assumed for the fourth stage. The validity of the preceding field will be lost after the time when the angle $\angle 14 \cdot 15 \cdot 16$ becomes zero, and thus the change of the field occurs.

In this new field, a parallel band zone constructed by lines 5·N·16 and $15 \cdot N_1 \cdot 6$ extends from the contact border points 6 and 16.

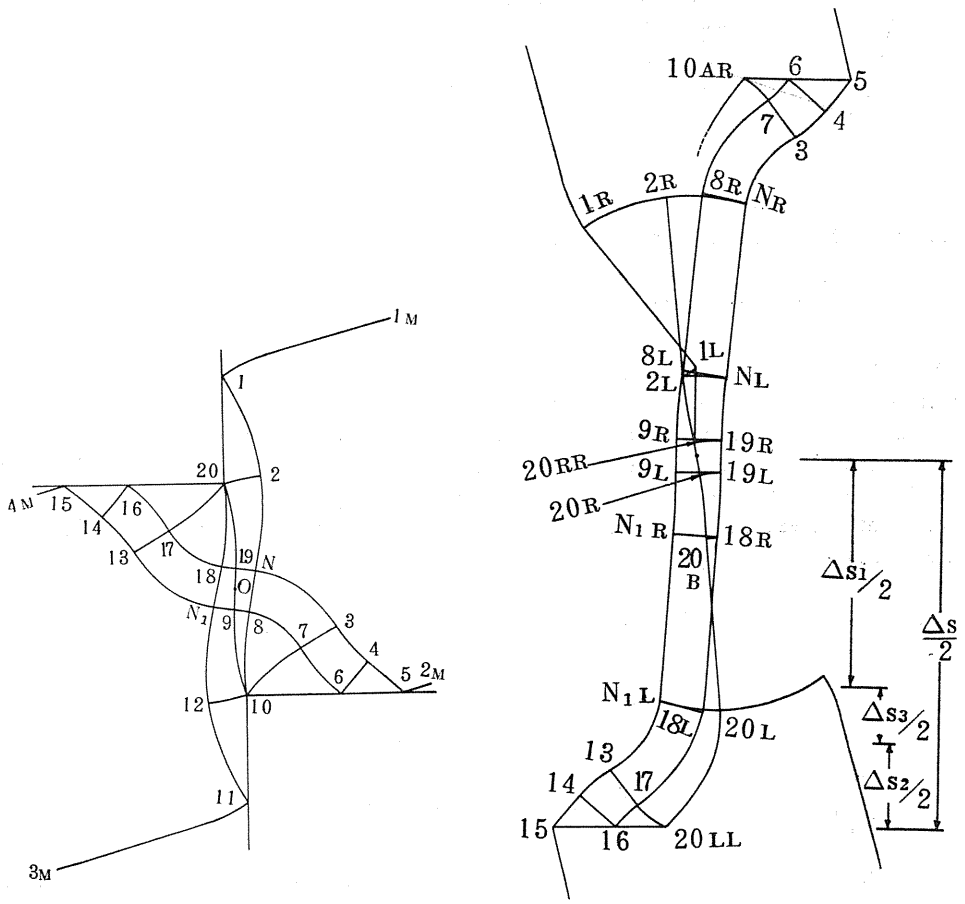

a. Physical plane b. Hodograph plane

Fig. 25. Slip-line field for the fourth stage.

4. Quantitative Analysis

Through this analysis, shape of the field and the hodograph were determined by means of an equilibrium equation and three stress boundary conditions.

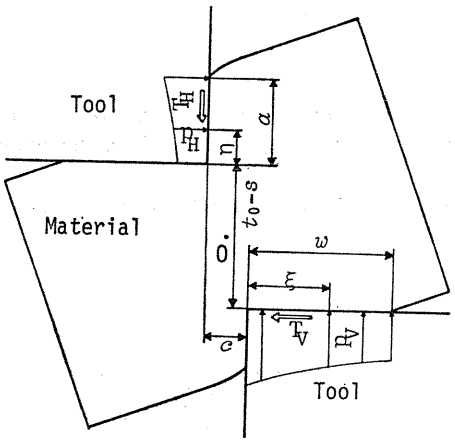

Fig. 26. External forces acting on the material.

As shown in Fig. 26, for an equilibrium of the external moments acting on the material, the following condition must be satisfied

$$\int_0^w p_V(2\xi+c)d\xi+T_H\cdot c=\int_0^a p_H(2\eta+t_0-s)d\eta+T_V(t_0-s) \qquad (3).$$

where ξ and η are the coordinates of the element on the tool face and on the mantle respectively, referring to the edge.

In the fields of Figs. 23, 24 and 25, the following three equations must be satisfied for the sake of equilibrium of the stresses acting on the rigid portions. In these equations the symbols used are; N: the origin of the coordinates, p_0: the hydrostatic pressure and φ: the inclination of the β-lines measured clockwise from the y-axis.

$$\int_{(\alpha)} p_0\cdot dy-\int_{(\beta)} p_0\cdot dy+\int_{(\alpha,\ \beta)} k\cdot dx=0, \qquad (4)$$

$$\int_{(\alpha)} p_0\cdot dx-\int_{(\beta)} p_0\cdot dx-\int_{(\alpha,\ \beta)} k\cdot dy=0, \qquad (5)$$

$$\int_{(\alpha)} p_0(ydy+xdx)-\int_{(\beta)} p_0(ydy+xdx)+\int_{(\alpha,\ \beta)} k(ydx-xdy)=0, \qquad (6)$$

where the integrations are carried out from the origin N to the surface along the N$\sim$5 on α-line and the N$\sim$1 on β-line.

Further, along the α- and β-lines Hencky's equation can be written as

$$p_0 = p_{0,N} \pm 2k(\psi - \psi_N), \tag{7}$$

where $p_{0,N}$ means hydrostatic pressure at the origin N and φ_N means the inclination of β-line there, and as for the double sign it must be positive along the α-line and negative along the β-line. Substituting Eq. (7) in Eqs. (4)～(6), we obtain the expressions for hydrostatic pressure $p_{0,N}$, the coodinates x, y and φ which determine the shape of the slip-line field.

As parameters necessary for constructing the slip-line field, c, e, w, and a are considered. They are again; — c: clearance, e: vertical gap of both edges, w: contact width, a: contact width of the tool mantle face, $k\cdot\cos 2\gamma$ and $k\cdot\cos 2\delta$: the frictional shear stresses on the tool face and the mantle face and $2k\zeta$: the difference of the pressures at the edge and at the contact border when their distribution on the tool face is assumed to be linear.

Now in constructing the field, γ, c, e and w are known, $p_{0,N}$, δ, ζ and a must be determined so as to satisfy Eq. (3)～Eq. (6). (see Appendix 2)

4. 1. Working load

The chain-lines in Fig. 27 show theoretical working loads obtained by the integration of the pressure on the tool face etc., where parameters of curves are clearance c and stress τ_V on the tool face. The solid-lines in the same figure show the experimental values obtained from aluminium A1100-H14, lubricated by Johnson-wax No. 151, and sheared with tools of different clearances. It will be seen that the theory agrees well with the experiment, so far as observing the change of tendencies of curves with the change of clearance. The smaller the clearance, the more rapidly the curve increases at the beginning, and the earlier the maximum point of the curve is reached.

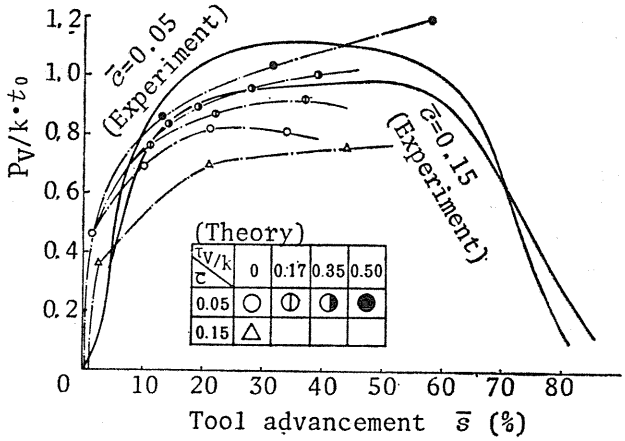

Fig. 27. Process of theoretical and experimental working loads.
[Experimental conditions, Specimen: Aluminium A1100-H14, Lubricant: Johnson-wax No. 151, Tools: Straigh square edges]

Since the working load reflects mainly the integration of pressure on the tool face, its process must be a result of balance of the increase of contact width and

the decrease of pressure with the tool advancement. However, as the contact width w can be estimated theoretically, the theoretical w 's were compared with the experiment. The result is shown in Fig. 28. The similar estimating process was applied to the pressure $p_{v,m}$. The result is shown in Fig. 29.

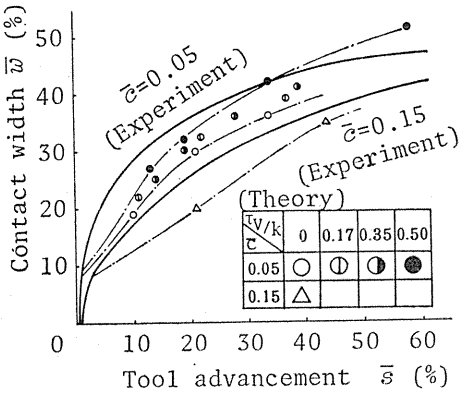

Fig. 28. Process of theoretical and experimental contact width.
[Experimental condition,
Specimen: Aluminium A1100-H14
Lubricant: Johnson-wax No. 151
Tools: Straight square edges]

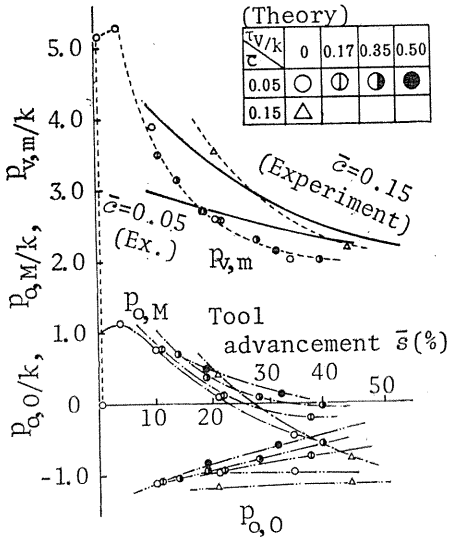

Fig. 29. Processes of various pressures.
[Pv, m: Mean pressure on the tool face
Po, M: The minimum of hydrostatic pressure governing the material surrounding cutting edges
Po, O: The minimum hydrostatic pressure as a whole]

Referring to both figures one can explain the difference in tendencies of the loads due to working conditions in Fig. 28. For example, supposing that external forces satisfy equation (3), the change of the contact width w and that of load P_v due to clearance can be explained.

4. 2. Hydrostatic pressure in the neighborhood of cutting edge

Now, let us explain the various phenomena on the basis of theoretically estimated hydrostatic pressure. At first, Fig. 30 gives in three-dimensions the distribution of hydrostatic pressures prevailing in the material. In this figure, z-axis indicates the pressure where x-y plane corresponds to the sectional plane of the material. The clearance is 5%, the frictional shear stress τ_v is assumed to be $0.35k$ and the pressure at a stage of 19% is shown (for the sake of simplicity only a half of the zone is shown).

It will be realized that the pressure governing the material surrounding the cutting edge takes its minimum at the point M. The chain-lines in Fig. 29 show the process of this minimum hydrostatic pressure $p_{o,m}$ at that point together with

other pressures. It will be noticed from this figure that $p_{o,m}$ becomes negative immediately before the crack initiation.

The hydrostatic pressure, its minimum of all is reached in the neighborhood of the center O, the intermediate of both cutting edges. However, a crack does not initiate from that center region but from cutting edges as above. It may be concluded at least that the ultimate crack in the blanking operation is caused not only by a tensile state of the mean stress. Double dotted dash lines in Fig. 29 show the process of the hydrostatic pressure $p_{o,o}$ at the center O. They appear to be always negative so that the stresses there are always tensile throughout a process.

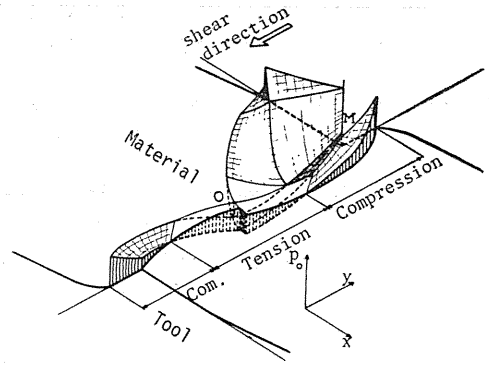

Fig. 30. Hydrostatic pressure distribution in the material estimated by the slip-line field technique.

The broken lines in the same figure show the theoretical values of the mean pressure $p_{v,m}$ on the tool face, and the solid-lines in comparison show corresponding experimental values which are the measured load divided by the contact area.

5. Summary

In the preceding part, the scissors type shearing has been regarded as a copybook which can include fundamental phenomena in many shearing processes of practical use. In this part, an attempt made to establish the kinematics of this process has been presented. A description has been given of a consistent image of this process using slip-line fields and some assumptions for the sake of simplicity. Conclusions are as follows.

(1) Four fields of different patterns, which correspond to stage developed in a process, have been proposed. They could transit one by one consistently through a process offering a clear interpretation of the shearing mechanism.

(2) The slip-line fields proposed, being characterized by a consideration of material rotation, seem to be more rigorous in the plasticity theory than any other models so far, so they appear to explain more clearly the deformation in a real process.

(3) The slip-line field and the relating hodograph have been newly constructed which are completely compatible with the equilibrium of external forces and of the stresses acting on the rigid portions, being given the tool advancement, clearance and frictional stress on the tool face.

(4) The slip-line fields can be closely related to the analysis of the constituent components of the tool advancement proposed in the previous part, so the state of a process for a particular stage can be represented much clearer.

(5) The process of the working load estimated from the slip-line field technique agreed well with that of the experimental load.

(6) In this analysis, the change of the contact width and that of load with change of the clearance has been theoretically explained.

(7) It has been observed that hydrostatic pressure in the neighborhood of cutting edge becomes negative immediately before the crack initiation.

(8) It appears that the ultimate crack is caused by not a state of positive hydrostatic stress alone but also by state of other factors such as total strain, strain path length, stress history and so on.

Appendix 1. Increase of the Contact Width w at the Beginning of the Process

The process of forming the contact width w in the first stage (Fig. 22), is obtained on the basis of the equation (3) which expresses the equilibrium of the external forces.

Substituting $p_V=2k\left(1+\frac{\pi}{2}+\omega\right)$, $p_H=2k(1+\omega)$, $T_V=T_H=0$ and $a\simeq s-t_0(1-\cos\omega_s)$ into the equation (3), we obtain

$$w^2+c\cdot w-A\cdot s=0, \tag{8}$$

where

$$A=t_0\cdot\cos\omega_s\cdot(1+\omega)/\left(1+\frac{\pi}{2}+\omega\right).$$

From equation (8), the partial derivative of w with respect to s can be expressed as follows,

$$\partial w/\partial s=A/(2w+c). \tag{9}$$

In the first stage, $\partial w/\partial s$ is estimated at $8\sim2$ in case of $c=0.05$ and $\partial w/\partial s=3\sim1$ in case of $c=0.15$.

The initial curves of the contact width were drawn, on the basis of w calculated from the equation (8), which is expressed as follows,

$$w=-\frac{c}{2}+\sqrt{\frac{c^2}{4}+A\cdot s}\ . \tag{10}$$

Appendix 2. Determination of the Hydrostatic Pressure p_0 and the Fields' Shape in Case of Figs. 23, 24 and 25

For example, calculation will be carried out in case of Fig. 24, provided that one fiftieth of the contact width w is assumed to be a unit length.

Substituting Eq. (7) in Eqs. (4) and (5), we obtain

$$\frac{p_{0,N}}{k}\left(\int_{(\beta)}dy-\int_{(\alpha)}dy\right)=2\int_{(\alpha,\beta)}(\psi-\psi_N)dy+\int_{(\alpha,\beta)}dx \tag{4}'$$

and

$$\frac{p_{0,N}}{k}\left(\int_{(\beta)}dx-\int_{(\alpha)}dx\right)=2\int_{(\alpha,\beta)}(\psi-\psi_N)dx-\int_{(\alpha,\beta)}dy \tag{5}'$$

Integrands of the first terms in the right-hand sides of Eqs. (4)' and (5)' are expressed in Fig. 31. These figures show inclinations of the β-(N$\sim$1) and the

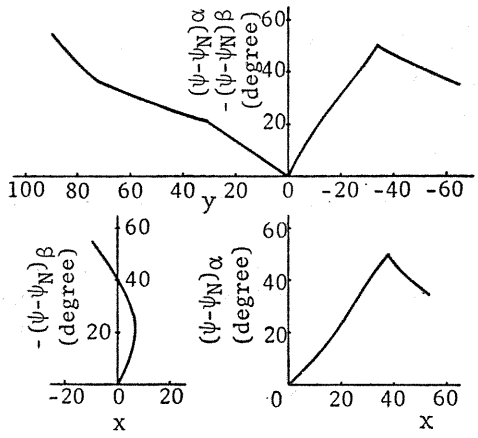

Fig. 31. Inclination of β-(N~1) and α-(N~5) lines in the field of Fig. 24.

α-(N~5) lines in terms of the angular difference of inclination at the regarding point and that at point N in Fig. 24 a. This field should really be constructed by giving prescribed values of $e=135$ units, $c=8.5$ units and $w=50$ units for linear dimensions and $\gamma=35°$ for inclination of β-shear line. In that, the contact width a, the inclination of β-line at mantle face δ and the pressure difference parameter ζ are indeterminable in the first place.

Referring to Fig. 31 integrating graphically $(\psi-\psi_N)$ with respect to x and y,

$$2\int_{(\alpha,\ \beta)}(\psi-\psi_N)\mathrm{d}y=-158.8,\quad 2\int_{(\alpha,\ \beta)}(\psi-\psi_N)\mathrm{d}x=70.4,$$

The ranges of integrations give

$$\int_{(\alpha,\ \beta)}\mathrm{d}x=39.5,\quad \int_{(\alpha,\ \beta)}\mathrm{d}y=25,$$

$$\int_{(\beta)}\mathrm{d}y-\int_{(\alpha)}dy=155\ \text{ and }\ \int_{(\beta)}\mathrm{d}x-\int_{(\alpha)}\mathrm{d}x=-58.5.$$

By substituting these values in Eqs. (4)′ and (5)′, two different values of hydrostatic pressure $p_{o,\,N}$ are attained as follows,

$$p_{o,\,N}/k=-0.770\quad\text{from}\quad\text{Eq. (4)}'$$

and

$$p_{o,\,N}/k=-0.776\quad\text{from}\quad\text{Eq. (5')}.$$

These values are regarded as a good approximate and simultaneous satisfaction of the both equations.

Now, estimating $p_{o,N}/k$ at -0.773 and by utilizing Eq. (7) etc., equation for the pressure on the tool face is obtained as: $p_V/k=3.20-0.02\xi$ and for the pressure on the tool mantle: $p_H/k=1.20+0.05\eta$.

Thus, the value of terms in Eq. (3) which expresses the equilibrium of the external moment come to be calculated as follows:

the first term of left-hand side $=\int_0^{50}k(3.20-0.02\xi)(\xi+8.5)\mathrm{d}\xi=7370k$,

the second term of left-hand side $= 117k$,

the first term of right-hand side $=\int_0^{21} k(1.02+0.05\eta)(134+\eta)\mathrm{d}\eta=5239k$,

and the second term of right-hand side $=2278k$,

so, the left-hand side $= 7370k+117k=7487k$

and the right-hand side $= 5239k+2278k=7517k$.

Consequently, it would be recognized that the left-hand side $\simeq$ the right-hand side. Similarly, whether Eq. (6) holds or not can be examined.

The above trial calculations should be repeated until an agreement of hydrostatic pressures $p_{o,N}$ s from Eqs. (4)′ and (5)′ is attained and at the same time Eqs. (3) and (6) are satisfied. In this way, plausible values of $p_{o,N}$, a, δ and ζ are determined.

Part Ⅲ. Material Flow in the Deformation Zone of the Metal Subjected to Blanking with Tools Having Closed Contours[41]

1. Introduction

As a number of engineering components come to be produced from sheet metals or plates by so called precision types of the blanking[7], general and proper understanding of the mechanism of blanking has become urgent for making the processes successful. Though the process of deformation in the shearing operation has been studied by many investigators so far, analyses are confined to the condition of plane strain.[21~25] In the preceding two parts of this investigation also, the process under the condition of plane strain was dealt with. However, since a blanked component usually takes a closed contour, the existence of the contour's curvature makes the shearing process complicated.[15, 20, 29~31] Difficulty in analysis arises partly from the preparation of test specimens which can be sectioned and reassembled in order to observe the deformation during the process. Researches so far could not be based on an actual behavior of metal flow as yet, because examinations of metal substrates before and affer a blanking had been so few.

Authors developed two kinds of new techniques by which the flow of metal during the blanking of closed contours could be studied. In this part, the mechanism of blanking based on the knowledge of the metal flow proved by these techniques will be described.

2. Experimental Method and Condition

Metal flow caused by advancement of the punch has been investigated in detail by blanking circular test specimens of aluminium with concentric circular tools. At first, the visioplasticity method was applied to the clearance zone by means of a grid photoetched on one of the meridio-sectional planes of the specimen halves. Then, in the neighboring of that zone strain gauges were applied on both surfaces in order to detect the surface strains of the specimen.

2. 1. Condition

The material tested was 4 mm thick half-hardened aluminium sheet from which circular blank specimens of 60 mm and 90 mm dias. were prepared by an engine lathe. The mechanical properties of test material are shown in Table 4.

Table 4. Mechanical properties of test material.

Method	Visioplasticity	Strain gauge
Material	Aluminum (A1100P-H14)	
Thickness mm	4	
Diameter mm	60	60, 90
0.2% proof stress kgf/mm^2	10.20	13.85
Ultimate strength kgf/mm^2	10.83	15.03
Strain hardening factor	0.031	0.038
Uniform elongation %	3.2	2.8

For testing, specimens were centrally pierced with 8 and 20mm dias. tool sets so as to leave blanks of due diameters. When utilizing specimens of 90 mm dia.

Table 5. Experimental conditions.

[Tool]	Visioplasticity	Strain gauge
Diameter mm	8, 20	20, 50
Material	SKD 11 (hardened, ground)	
Hardness (HRc)	60~63	
Roughness (R_{max}) μm	1.6	

Clearance: 0.25%, 3%, 6%, 20% of specimen thickness
Lubricant: Johnson-wax No. 151
Punch speed: 0.25mm/sec
Support: free

[Strain gauge method]
Properties of strain gauge
Gauge length: 1 mm
Gauge factor: 2.05
Gauge resistence: 120.2Ω ±0.03%

Measured radial distance (upper and bottom surfaces) mm	Tool dia. mm	Specimen dia. mm
1.5, 3, 16, 22	20	60
8, 15, 33, 39	50	90

tools of 50 mm dia. were used also.

The diameters of punches were of prescribed sizes, the die holes being ground so as to accommodate clearances to punches. Four kinds of clearances shown in Table 5 were tested.

The lubricant was Johnson-wax No. 151 and it was applied on both surfaces of specimens.

As regards the experimental conditions, see Table 5.

2. 2. Visioplasticity

At the time of applying visioplasticity, the specimens should be prepared so as to protect themselves from splitting due to the hoop tension during a process, this scheme is illustrated in Fig. 32. By means of this preparation, deformation of material in the clearance zone has been made clear for the first time.

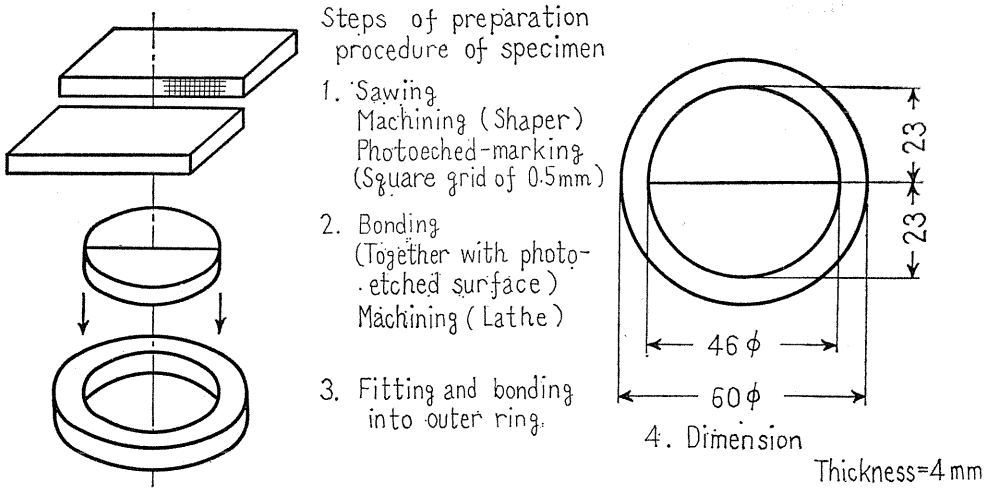

Fig. 32. Preparation procedure of specimen for visioplasticity.

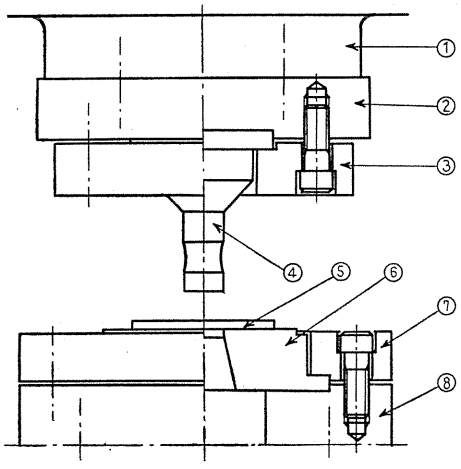

Fig. 33. Scheme of the experimental tool set.
1. diaphragm
2. 3. punch-holder
4. punch
5. specimen
6. die
7. 8. die-holder

Fig. 33 shows the tool set for this experiment, which was set in a four pillars type die-set and a gear driven press.

The punch load was measured by means of strain gauges bonded on the diaphragm ①, and was registered against punch stroke by an x-y recorder in which the stroke was detected by means of a potentiometer on one of the punch stem. At any instant of interest the driving unit could be stopped by a magnet-switch in which a contact point was placed beneath the bottom face of the punch holder ③. Thus, a distorted grid pattern on the section at that instant could be frozen and observed.

2. 3. Strain gauge method

In order to know the elastic or elastic-plastic behaviour of metal in the neighborhood of the clearance zone, the components of strain ε_θ, ε_r were measured by strain gauges bonded on the upper and bottom surfaces of specimen from which radial flow of metal was calculated.

For this purpose the upper tool shown in Fig. 34 has a central recess and holes which allow the lead wires to pass through.

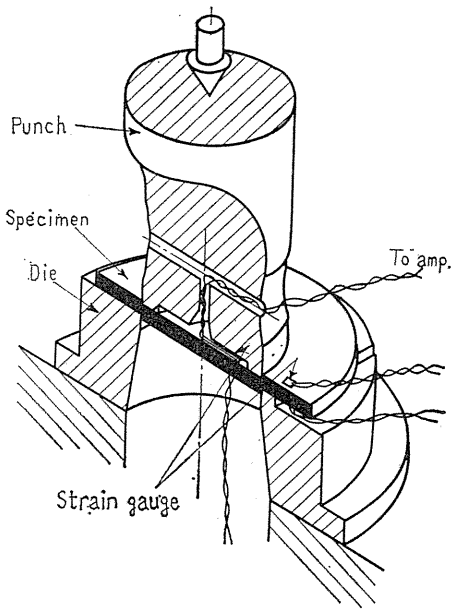

Fig. 34. Tools for strain gauge method.

3. Experimental Result and Consideration

3. 1. Region of the main deformation in the circular blanking

Fig. 35 shows a distorted grid pattern on the meridian section at the mid way of a blanking process, where the punch penetrated up to 40 % of metal thickness. The tools had 20 mm dia. and 0. 25 % clearance.

Fig. 36 shows the change of the deformation zone in the various clearances where the punch diameter is 20 mm and the stroke 10 %. The elastic-plastic boundary was obtained by means of plotting the position at which the horizontal grid line starts distortion. Severe deformation zones whose shapes are lenticular in general are shown blacked. These figures cleary show that, the smaller the clearance, the narrower become the widths of the severe deformation zone as well as the whole deformation zone.

Now, it will be desirous to see to what extent the deformation zone varies under the influence of tool's contour. Fig. 37 shows the change of the deformation

zone in the various specific curvatures t_0/R, which would be thought representing the severity of the configuration, where the clearance is 6 % and the penetration 20 %. In the circular blanking ($t_0/R \neq 0$), the material situating around the deformation zone constraints the radial displacement of the metal to flow into or out of the essential deformation zone, so, the deformation of the material in a pressed portion on the tool face does not seem to take place. A marked constrast to this

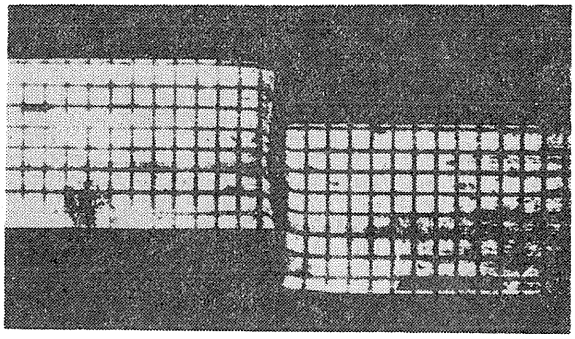

Fig. 35. Distorted grid pattern.

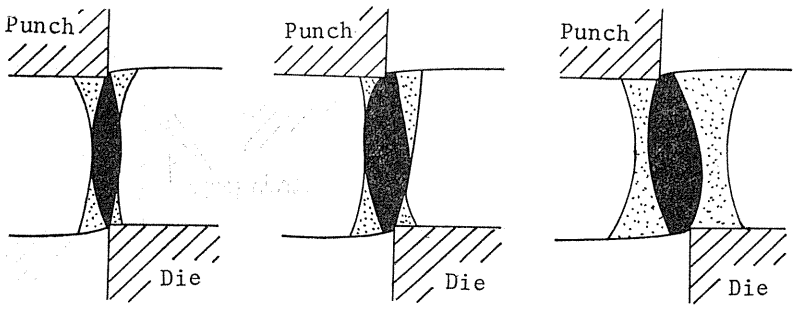

Clearance 0.25% 6 % 20%

Fig. 36. The region of the main deformation in various clearances.

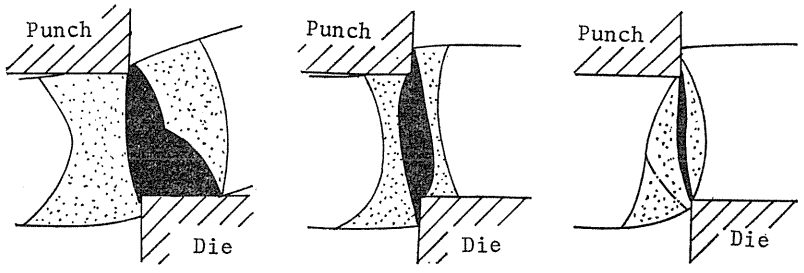

Plane strained shear with the scrap unconstrained $t_0/R=0$

Punch dia. ϕ 20 $t_0/R=0.4$

ϕ 8 $t_0/R=1.0$

Fig. 37. The region of the main deformation in various curvature of the blanked contour.

is observed in the two-dimensional shear process ($t_0/R=0$) where the material exposed to the pressed portion is deformed undergoing a machining-like separation. This figure shows that, the smaller the punch diameter, *i. e.*, the larger the curvature of the blanked contour, the narrower the deformation zone on the die.

The consideration so far leads to the following conclusion. The curvature of the blanked contour as well as the clearance are main influential factors to the blanking process. The mode of the deformation in the main region is influenced by these two factors, and the degree of the influence appears to depend on how the factors control the radial flow of the metal.

3. 2. *Severity of deformation*

In the analysis of metal flow by means of distorted grid pattern as Fig. 35, positions of the grid points were specified by $r-z$ coordinates shown in Fig. 38.

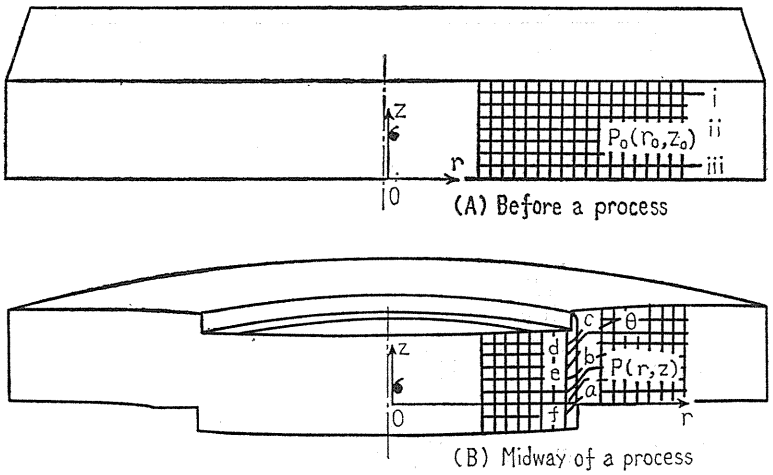

Fig. 38. Specification of position of grid points.

Fig. 39 shows the inclination θ of three originally horizontal lines when the punch penetrated 20 % of thickness. Before the process they passed through i, ii and iii of Fig. 38 (A). The tool had 20 mm dia. and clearance of 6 %. The abscissa shows the radial distance of the metal at that time. The maximum of θ appears to take place along the line i which lies nearer to the punch face. The lines i and iii lying beneath surfaces incline considerably in the rolled over portion near each cutting edge. These tendencies are observed also in cases of 0.25 % and 20 % clearances.

Fig. 40 shows θ's for different clearances, the punch diameter and the penetration being the same as above. It should be noted that, the smaller the clearance, the narrower the zone of plastic deformation and the larger the θ, so the strain in consequence.

3. 3. *Metal flow in the plastic zone*

In order to trace the metal flow, displacement of a material point was represented by the displacement vector PP_0 whose magnitude could be calculated by

subtraction of the original coordinates (r_o, z_o) of the point P_o shown in Fig. 38 (A) from the coordinates (r, z) of that point after deformation P.

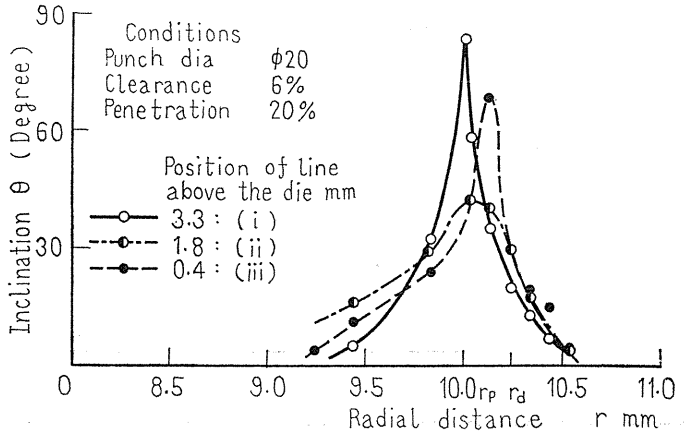

Fig. 39. Inclination of three originally horizontal lines
rp: radial distance along the punch
rd: radial distance along the die

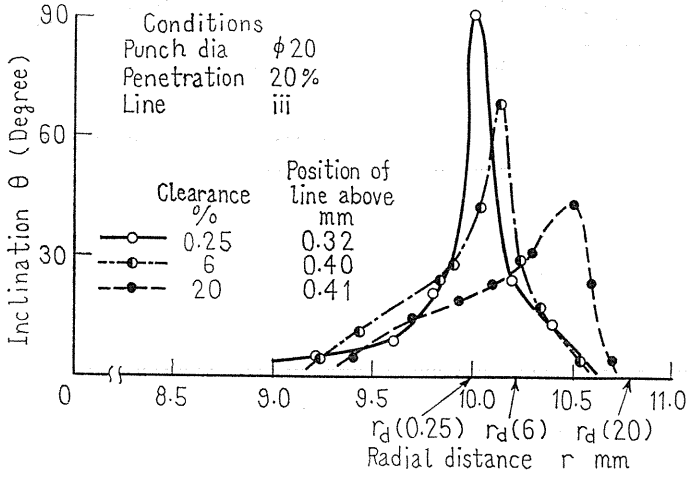

Fig. 40. Inclination of the line lying near the punch for different clearances. [r_d represents the position of die edge, figure in the bracket means clearance]

Fig. 41 shows the traces of metal flow in the typical regions of a to f shown in Fig. 38 (A). Points 2, 3 and 4 correspond to the positions at the punch penetrations of 10, 20 and 30 % respectively. It will be observed that at start of the penetration the radial component is centrifugal throughout the regions. This kind of centrifugal flow was always observed within the conditions of this experiment, though this flow seemed to decrease with clearance.

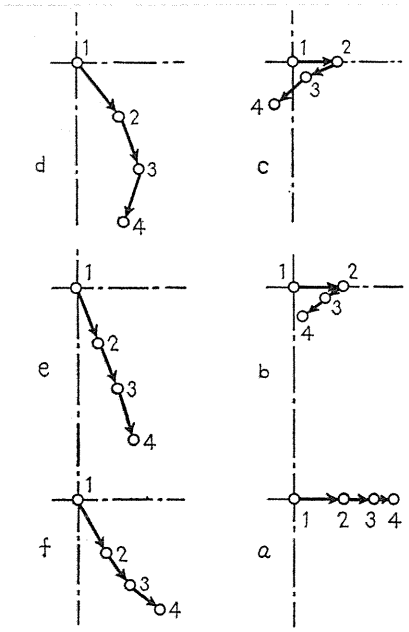

Fig. 41. Material displacements in the plastic zone.
Tool dia.=20mm, $c/t_0=0.25\%$

In the following, attention will be paid to the radial flow, because it seems to characterize the mechanism of blanking. The constraint due to a closed contour has influence on this and by knowing this flow out of or into the clearance zone one could tell the relative hydrostatic pressure of that zone to the neighborhood where no external force acts.

Increments of the radial displacements of the metal due to a incremental advancement of the tool are shown by the vectorical arrows and contour lines in Fig. 42 where a sequence of three typical stages is presented, the distributions being in accordance with deformed states and with the tool diameter of 20mm and the clearance of 20 %. The value subscript in the figure shows ratio of the displacement increment to the penetration increment.

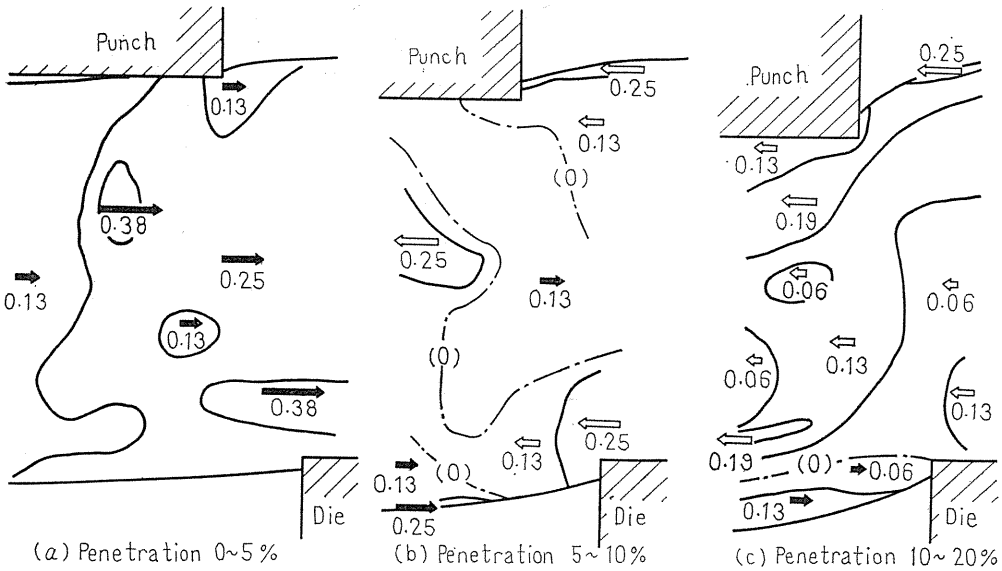

Fig. 42. Distribution on the radial flows in the plastic zone.

3. 4. Elastic deformation of metal in the neighborhood of the plastic zone

Fig. 43 shows development of the radial flow by v's at the gauging points.

The flow $v=\partial u/\partial s$ can be obtained as an inclination of the displacement u against penetration s curve, in that, the displacement u can be known with the aid of the equation $u=\varepsilon_\theta \cdot r$, from the strain ε_θ being measured by gauges bonded on the upper and bottom surfaces of the material. Broken line shows the average translation velocity $\tilde{v}$ over the thickness at those points. The positive sign of ordinates corresponds to the centrifugal flow.

The attendant sketch illustrate the distributions of the plausible radial velocities over the thickness estimated by these v's. It will be observed at the penetration of 5% that in both the product side and the scrap side, the material near the unconstrained surface flows into, and that near the pressed surface flows out from, the clearance zone. When the amount of penetration of the punch reaches 20%, the metal flow of the product side seem to almost cease. It will be observed that, at the time when the punch penetrates up to 30% just before the crack initiation for ultimate cleavage, the material wholly flows from scrap side into the clearance zone.

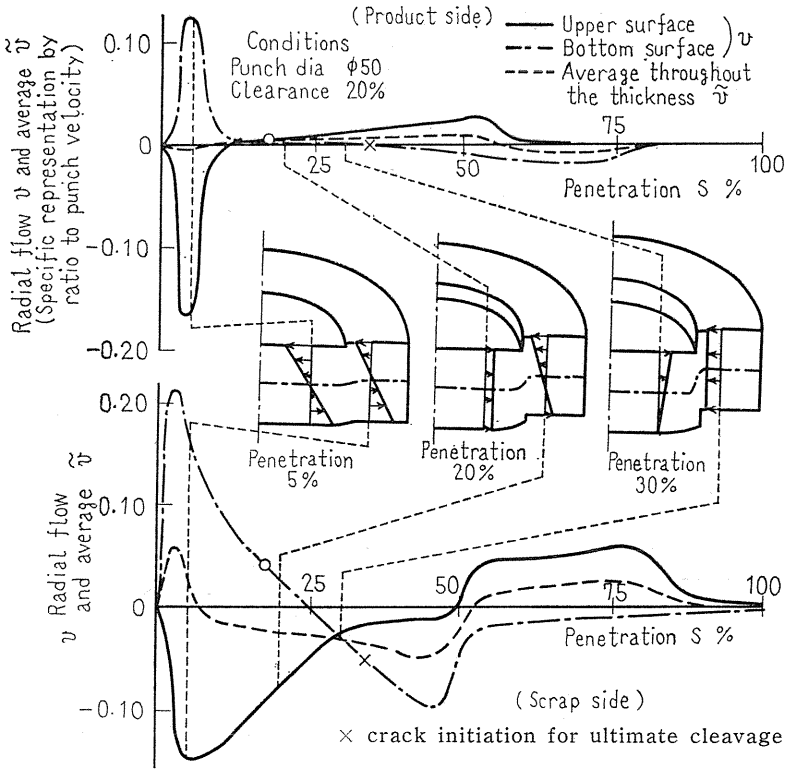

Fig. 43. Radial flow in the elastic zone.

3. 5. *Analysis of flow by a virtual displacement of the tool*

In this section, a new expression of deformation modes in the blanking will be proposed according to the above measurements.

In many researches so far, the velocity diagram has been generally so con-

structed that velocity vectors represent, so to say, the absolute ones which would be right when one considers that either the punch or the die stands still. In such a velocity field, difficulty arises in finding the boundary regions of elastic and plastic deformations, because in the material region being taken along with the moving tool every vector comes to have a dominated vertical component as shown in Fig. 41. The difficulty will be decreased by the following treatment.

Fig. 44 illustrates the method. At a particular stage of penetration, suppose

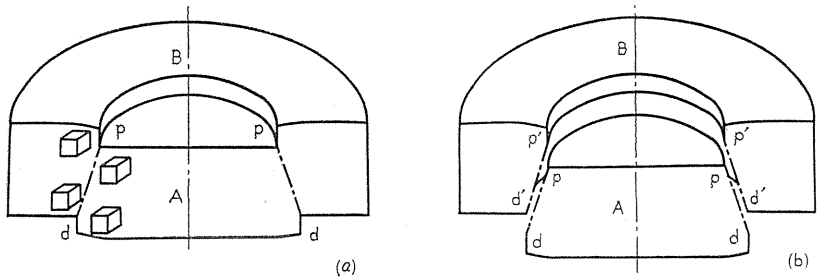

Fig. 44. Explanation of displacement of the assumed rigid material.

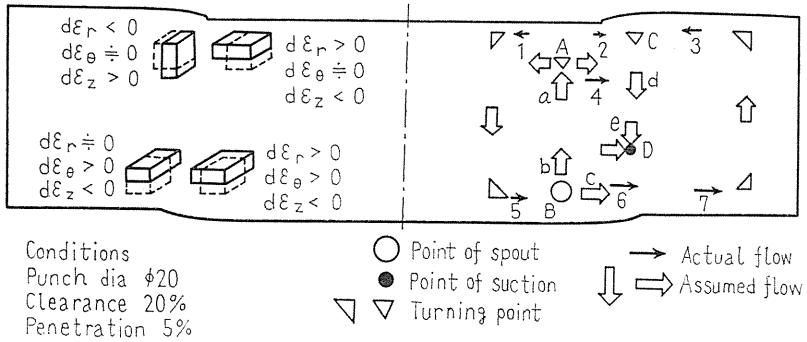

Fig. 45. Analysis of flow by a virtual displacement of the tool (penetration 5%)

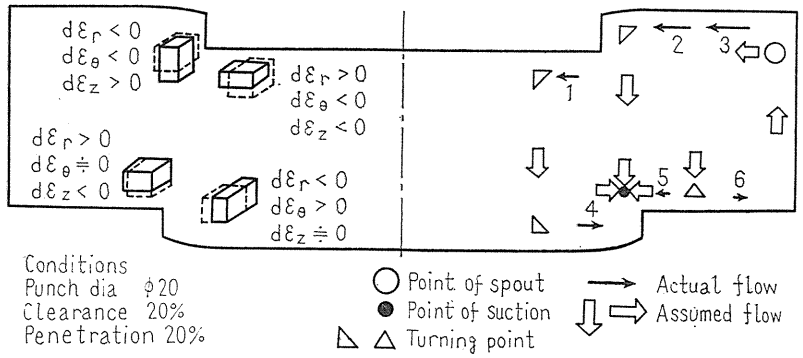

Fig. 46. Analysis of flow by a virtual displacement of the tool (penetration 20%)

that the specimen is cut off into two rigid pieces A and B separated by a conical surface joining the contour *pp* of the punch edge to the contour *dd* of the die edge. That state is shown by (a) of the figure. As the movement of the tool continues, and as shown in (b) of the figure, after an infinitesimal small advancement of it, the metal-flow in the vicinity of the virtually cut faces would be such that materials separated tend to flow from subsurfaces into the newly generated vacant space *p'd'pd*. Thus, four cubical elements shown in (a) of the figure should be subjected to due strains. Into this consideration, the velocities of the moving tool could not enter. The state of metal flow at the penetrations of 5% and 20% are shown in Fig. 45 and 46. The small arrows *1*, *2*, 3 etc., which represent the radial velocities, are written taking account of foregoing results. Here, a supposed point in the vacant space around which the material gathers would tentatively be called the 'point of suction', and the portion near the rolled over surface which can supply the material so as to fill the vacant space be called the 'point of spout'. The place where the direction of flow changes from axial to radial or *vice versa* would be called the 'turning point'.

Let us consider the state of the penetration of 5% shown in Fig. 45. The pressed portion *A* beneath the punch is regarded as a turning point, because the flow *a* should exist for the flows *1* and *2* to occur. On the other hand, in the pressed portion on the die almost no axial flow can be recognized because the difference between vectors *7* and *6* is negligible. The rolled over portion *B* in the product side would be regarded as a point of spout, since the existence of flow *b* is necessary for the above-stated *a* to occur and the flow *c* originates from the acceleration of the flow *5* to *6*. Conversely the rolled over portion *C* of the scrap side must be a turning point, because an axial flow *d* should occur by the flows *2* and *3*. Consequently the rolled over of the scrap is smaller than that of the product side.

After all, in the vicinity of the die edge, the material finds itself a situation of more scarcity than in that of punch edge. Thus it will be said that the hydrostatic pressure in the vicinity of the punch edge is higher than the other and the point of suction *D* should be located in the neighborhood of the die edge.

In the penetration 20% shown in Fig. 46 the point of suction moves still closer to die edge, so that the hydrostatic stress in the vicinity of the die edge becomes more tensile than before. In this case, a point of spout must locate on the outside of the specimen. In the left-halves of both figures, the incremental strains of the originally cubic elements at the respective penetrations are presented.

3. 6. Influence of the clearance on the radial flow

Fig. 47 shows the distribution of the average translational velocity $\tilde{v}$'s, along a radial line at two stages. Those near the clearance zone were estimated from extrapolations of distribution curves. The v^* shown in the figure represents the discontinuity of $\tilde{v}$ between the scrap side and the product side, and is regarded as one of the measures which express the flow into or out of the clearance zone. Fig. 48 shows v^* vs. s curves for various clearances, where the positive sign of v^* means the out flow from the clearance zone. It is shown in the figure that if the v^* curve passes through the negative region more, the crack of ultimate cleavage seems to initiate with a less penetration. This result implies that the clearance is an eminent factor having serious influence on the crack initiation.

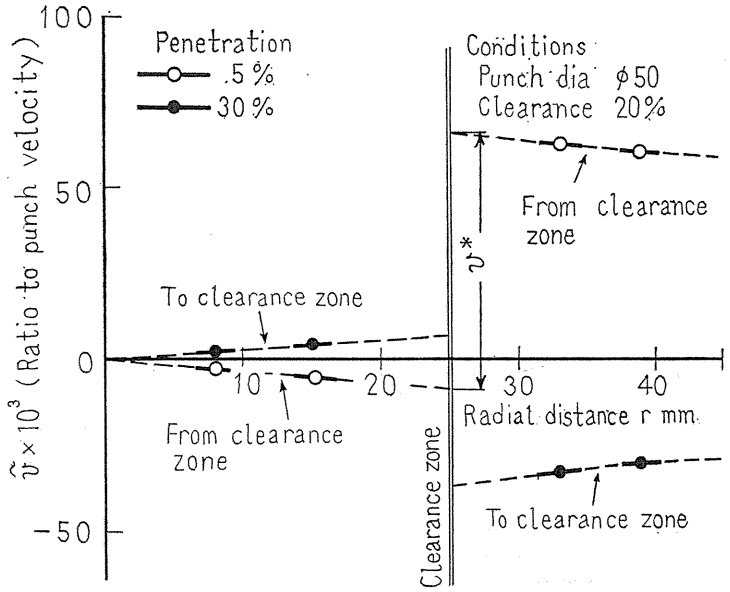

Fig. 47. Distribution of $\tilde{v}$ and definition v^*.

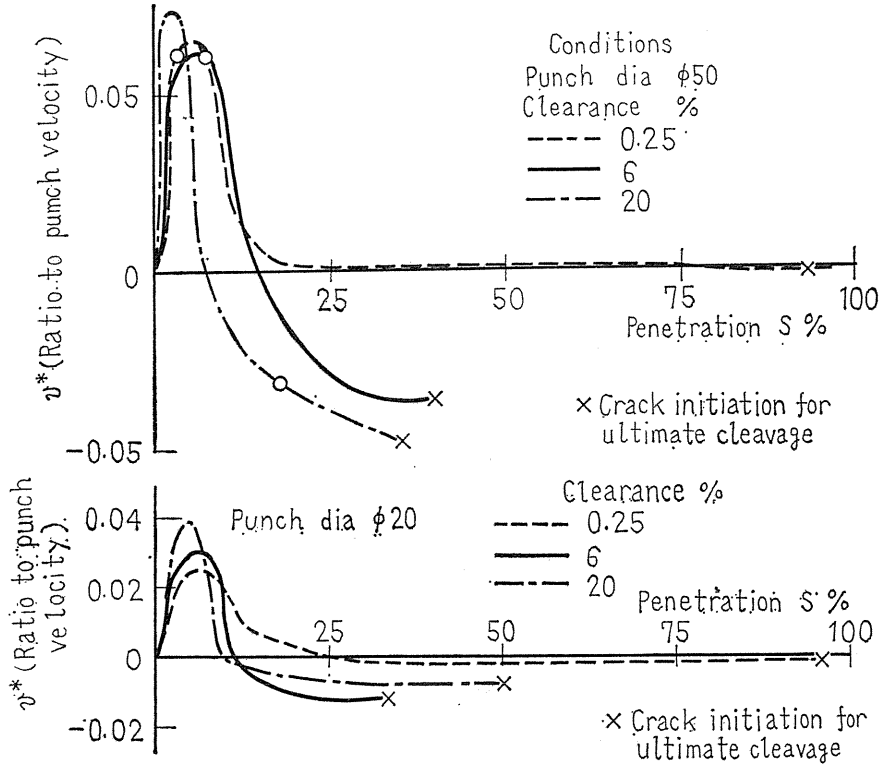

Fig. 48. Process of the discontinuity of velocity v^*.

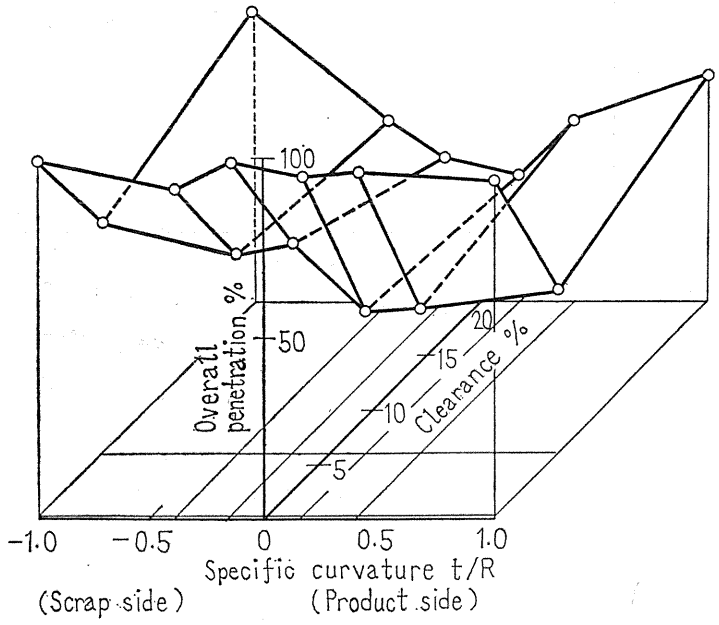

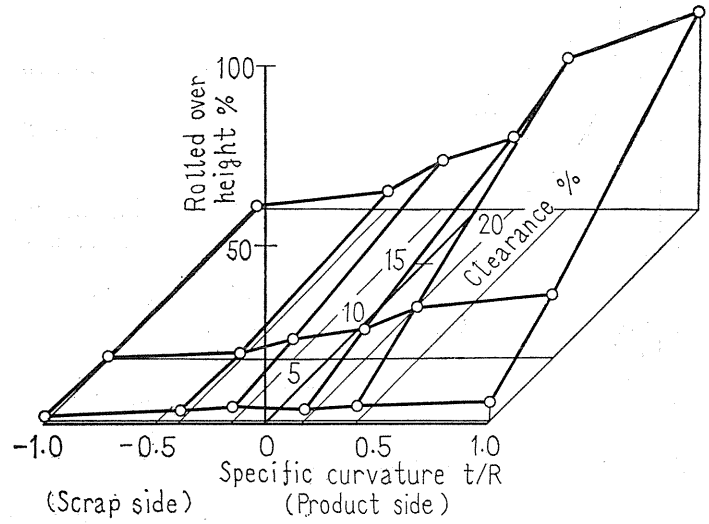

Fig. 49. Quality of the surface separated.

3. 7. Quality of the surface separated

Fig. 49 shows three-dimensionally the rolled over height and the overall penetration on a blanked contour-clearance plane, in that, the upper figure represents the summation of the rolled over, the sheared and the pressed heights. It expresses the penetration at crack initiation. The specific curvature and the clearance, composing two axes of the plane, will be taken as measures of the degree of the constraint which influences the blanking process under various conditions. It will be observed that due to the hydrostatic pressure mentioned in the previous section, the overall penetration seems to increase with smaller clearance. It can be seen readily that, the larger the specific curvature, the higher the rolled over, and, the larger the clearance, the more eminent will be this tendency. The result corresponds to the existence of the point of spout at B shown in Fig. 45.

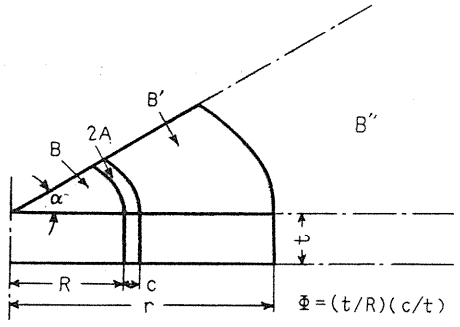

Fig. 50. Definition of the degree of constraint.
R: punch radius
r: specimen radius
c: clearance
t: thickness
2A: deficient volume in clearance zone
B: volume under the punch
B': volume on the die
B'': influential volume on the constraint

The degree of constraint could, in principle, be described as follows. In Fig. 50, the clearance volume is defined as $\alpha R t_0 c$. And in a blanking process, this volume would be considered a deficient volume to be replenished by the neighboring material. Severity in this material supply governs the flow and this should bring about the so called constraint. So, degree of constraint ϕ may be expressed as a ratio of the half of clearance volume which can be supplied. In this figure, for example, the material under the punch is considered as the volume to supply, the degree of constraint would be expressed by

$$\phi \text{ (degree of constraint)} = \mathrm{A/B} = (\alpha R t_0 c/2)/(\pi R^2 t_0 (\alpha/2\pi))$$
$$= t_0/\mathrm{R} \text{ (specific curvature)} \times c/t_0 \text{ (specific clearance)}$$

4. Summary

An experiment has been carried out for studying the flow of metal during the blanking of closed contours. Results are as follows:

(1) By means of a newly applied visioplasticity on the meridio-sectional plane

of the specimen, the behavior of metal flow, which has been guessed so far, is clarified in detail.

(2) In addition to the knowledge of the visioplasticity, by using the strain gauges applied to detect the surface strains of specimen, the metal flow throughout the whole specimen even in the elastic region could be taken into account.

(3) By aid of the flow analysis on the basis of the virtual displacement of the punch, it has become clear that, at start of a process the rolled over arises more in the product side than in the scrap side. And, in the process the position of the lowest hydrostatic pressure appears to move closer to the die edge.

(4) The analysis of the metal flow into or out of the clearance zone has revealed that, as the clearance becomes larger, the danger of crack initiation at less penetration increases.

Acknowledgement

The authors wish to thank Mr. Y. Matsuo and Mr. N. Hirabayashi for their kind cooperation in conducting the experiments in this part.

References

1) Crane, E. T.: Machinery and Production Engineering, No. 30 (1927), pp. 225.
2) Crane, E. V. & Edward, V.: Plastic Working in Presses, (1957) Willey, pp. 25~80.
3) Krabbe, E.: Stanzreitechnik, Maschinenbau, No. 15 (1936-10).
4) Iliescu, C., Tureac, I. & Gaspar, L.: Genau-Scherschneiden von Stangen, Werkstatt u. Betrieb, Vol. 110, No. 10 (1977), pp. 689~696.
5) Everett, J.: Fully automated feeding equipment for the high-speed, precision cropping of bar stock, Metallugia and Metal Forming, (1976-2), pp. 55~59.
6) Lawson, R.: Cropping billets fo cold extrusion, ibid., pp. 40~47.
7) Guidi, A.: Some current developments in the fine-blanking process and its tooling — Part 1, Sheet Metal Industries, Vol. 46, No. 1 (1969), pp. 41~52.
8) Ibid.: ibid. — Part 2, ibid., Vol. 46, No. 2 (1969), pp. 131~148.
9) Ibid.: Stanzreitechnik, Nachschneiden und Feinstanzen, Werkstatt u. Betrieb, Vol. 94, No. 11 (1961), pp. 843~849.
10) Scheuermann, H.: Maβnahmen zum Verbessern der Scherflachengute von Stahlknuppeln, Ind. -Anzeiger, 97. Jg. Nr. 69 v. 29. 8 (1975), pp. 1538~1544.
11) Kienzle, O. & Jordan, Th.: Messugen der beim Lochen von Blechen auf ein Schnittwerkzeug wirkenden Schnittkräfte, Mittelteilungen der Forschunggesellschaft Blecheverarbeitung, 19 (1954), pp. 218~219.
12) Cook, M. & Richards, T.: The tensile/shear stress ratio in rolled copper alloys, Journal of the Institute Metals, 73 (1947), pp. 541~551.
13) Chang, T. M. & Swift, H. W.: Shearing of Metal Bars, ibid., 78 (1950 1951), pp. 119~146.
14) Chang, T. M. Shearing of Metal Blanks, ibid., pp. 393~414.
15) Timmerbeil, Fr. W.: Der Einfluβ der Schneidkantenabnutzung auf den Schneidvorgang am Blech, Werkstattstechnik u. Maschinenbau, Vol. 46. No. 2 (1956), pp. 59~66.
16) Ibid.: Untersuchung des Schneidvorganges bei Blech, insbesondere beim geschlossenen Schnitt (Erster Teil: Der Schneidvorgang bei Scarfen Werkzeugkanten — die Schneidkräfte), ibid., Vol. 47, No. 5 (1957), pp. 231~239.

17) Ibid.: ibid. (Zweiter Teil: Die Schnittflächengute von Schnittteilen), ibid., Vol. 47, No. 7 (1957), pp. 306 ~356.
18) Kienzle, O. & Kienzle, W.: Werkzeugverschleiβ beim Schneiden vom Stahlfeinblechen, Stahl u. Eisen, Vol. 78, No. 12 (1958-12), pp. 820~829.
19) Wang, K. K., Taraman, K. & Wu, S. M.: An Analysis of Punching Variables by Two-Level Fractional Factorial Design, Journal of Engineering Industry, Trans. ASME, (1970-May), pp. 435~443.
20) Reichel, W. & Katz, R.: Das Stanzen Kleiner Locher, Blech, No. 1 (1968-1), pp. 24~34; No. 2 (1968-2), pp. 63~71; No. 3 (1968-3), pp. 115~130; No. 4 (1968-4), pp. 160~164; No. 5 (1968-5), pp. 260~269.
21) Jimma, T.: The Theoretical Research on the Blanking of the Sheet Material (Part 1, Analysis of the Statically Admissible Stress Field), Trans. Japan Soc. Mech. Engrs. (in Japanese), Vol. 28, No. 196 (1962-12), pp. 1638~1646.
22) Ibid.: ibid. (Part 2, Analysis of the Kinematically Admissible Velocity Field), ibid., Vol. 28, No. 196 (1962-12), pp. 1647~1654.
23) Ibid.: The Theoretical Research on the Blanking of a Sheet Material, Bulletin of JSME, Vol. 6, No. 23 (1963), pp. 568~576.
24) Kondo, K.: Mechanism of the Shearing Processes of Ductile Sheet Metals (1st Report) — Effect of the Mechanical Properties of aterial and Friction of the Tool Surfaces —, Jour. Japan Soc. of Precision Engrs. (in Japanese), Vol. 31, No. 6 (1965), pp. 38~45.
25) Maeda, T.: Theory of Shearing Mechanism for Sheet Metals with Punch and Die, Jour. Japan Soc. of Precision Engrs. (in Japanese), Vol. 25, No. 6 (1959), pp. 248~263.
26) Stromberger, C. & Thomsen, Th.: Glatte Lochwände beim Lochen, Werkstatt u. Betrieb, Vol. 98, No. 10 (1965), pp. 739~747.
27) Eickhoff, W.: Untersuchung über den Kraft- und Arbeitbedarf beim Lochen von Grobblechen, Werkstatt u. Betrieb, Vol. 94, No. 7 (1961), pp. 487~499.
28) Тимощенко, В. А.: Исследование и Разработка Способов Чистовой ВЫрубки и Зачистки с Осадкой Отхода, Кузнечно-Штамповочное Производство, No. 4 (1977), pp. 29.
29) Ozaki, T.: Preprint of 22nd Japanese National Conf. for Plastic Working (in Japanese), (1971-11), pp. 367.
30) Шенкар, В. С. & Шустицкий, Ф. М.: Исследование Очага Деформации Разделительньх Операций Штамповки, Кузнечно-Штамповочное Производство, No. 12 (1973-12), pp. 19 23.
31) Хмара, С, М., Смолянинов, В. П., Смирина, С. И. & Шевченко, М. М.: Течение Металла по Пояску Смятия при Вырябке, Кузнечно-Штамповочное Производство, No. 3 (1973-3), pp. 23.
32) Kasuga, Y., Tsutsumi, S & Mori, T.: On the Shearing Process of Ductile Sheet Metals (1 st Report, Experiment on the "Scissors Type" Shear), Bull. JSME, Vol. 20, No. 148 (1977-Oct.), pp. 1329 1335.
33) Tsutsumi, S.: Grid Technique and Analysis — Technique of Stress Analysis for Beginner (6) —, Jour. Japan Soc. for Technology of Plasticity (in Japanese), Vol. 13, No. 133 (1972), pp. 149 157.
34) Tamura, K. & Kudo, H.: Penetrating Force and Fracture Initiation in Cutting Cold-Rolled Pure Copper between Knife-Edged Tools — Study on the Cutting of Metal Strip between Knife edged Tools: 1st Report —, Jour. Japan Soc. for Technology of Plasticity (in Japanese), Vol. 7, No. 66 (1966), pp. 360 370.
35) Kasuga, Y., Tsutsumi, S & Mori, T.: On the Searing Process of Ductile Sheet Metals (2nd Report, Theoretical Analysis of the "Scissors Type" Shear), Bull. JSME, Vol. 20, No. 148 (1977-Oct.), pp. 1336 1343.
36) Bach, E. L.: Die Spannungen im Material unter einer Kreisringformigen Schnide, Diss., T. H. Karlsruhe (1924).
37) Krämer, W.: CIRP Annals (1968).
38) Тимощенко, В. А., Ермилов, В. В & Эрлих, А. И.: Исследование Деформирования Заго-

товки при Резке Сортового Проката Сдвигом, Кузнечно-Штамповочное Производство, No. 12 (1977), pp. 26.
39) El-Wakil, S. D.: Deformation in Bar Cropping Investigated by Visioplasticity, Journal of Mechanical Working Technology, No. 1 (1977), pp. 85～98.
40) Prager, W.: Problem der Plastizitatsthoris, Birkhauser, pp. 83～85.
41) Kasuga, Y., Tsutsumi, S. & Mori, T.: On the Shearing Process of Ductile Sheet Metals (Material Flow in the Deformation Zone of the Metal Subjected to Blanking with Tools Having Closed Contours), Bull. JSME, Vol. 21, No. 154 (1978-Apr.), pp. 753～760.